Search for gravitational wave signals from known pulsars in LIGO-Virgo O3 data using the 5n-vector ensemble method

Luca D'Onofrio,[1,*] Rosario De Rosa,[2,3] Cristiano Palomba,[1] Paola Leaci,[1,4] Ornella J. Piccinni,[5] Valeria Sequino,[2,3] Luciano Errico,[2,3] Lucia Trozzo,[3] Jim Palfreyman,[6] James W. McKee,[7,8] Bradley W. Meyers,[9] Ingrid Stairs,[10] Lucas Guillemot,[11,12] Ismaël Cognard,[11,12] Gilles Theureau,[11,12,13] Michael J. Keith,[14] Andrew Lyne,[14] Chris Flynn,[15] and Ben Stappers[14]

[1]*INFN, Sezione di Roma, I-00185 Roma, Italy*
[2]*Università di Napoli "Federico II," I-80126 Napoli, Italy*
[3]*INFN, Sezione di Napoli, I-80126 Napoli, Italy*
[4]*Università di Roma "Sapienza," I-00185 Roma, Italy*
[5]*Institut de Fisica d'Altes Energies (IFAE), The Barcelona Institute of Science and Technology,*
Campus UAB, 08193 Bellaterra (Barcelona), Spain
[6]*University of Tasmania, Hobart TAS 7005, Australia*
[7]*E.A. Milne Centre for Astrophysics, University of Hull,*
Cottingham Road, Kingston-upon-Hull HU6 7RX, United Kingdom
[8]*Centre of Excellence for Data Science, Artificial Intelligence and Modelling (DAIM), University of Hull,*
Cottingham Road, Kingston-upon-Hull HU6 7RX, United Kingdom
[9]*International Centre for Radio Astronomy Research (ICRAR), Curtin University,*
Bentley, Western Australia 6102, Australia
[10]*Department of Physics and Astronomy, University of British Columbia,*
6224 Agricultural Road, Vancouver, British Columbia V6J 2B1, Canada
[11]*Laboratoire de Physique et Chimie de l'Environnement et de l'Espace,*
Université d'Orléans/CNRS, F-45071 Orléans Cedex 02, France
[12]*Observatoire Radioastronomique de Nançay, Observatoire de Paris, Université PSL,*
Université d'Orléans, CNRS, 18330 Nançay, France
[13]*LUTH, Observatoire de Paris, PSL Research University, 92195 Meudon, France*
[14]*Jodrell Bank Centre for Astrophysics, Department of Physics and Astronomy,*
The University of Manchester, Manchester M13 9PL, United Kingdom
[15]*OzGrav-Swinburne University of Technology, Victoria 3166, Australia*

The 5n-vector ensemble method is a multiple test for the targeted search of continuous gravitational waves from an ensemble of known pulsars. This method can improve the detection probability by combining the results from individually undetectable pulsars if few signals are near the detection threshold. In this paper, we apply the 5n-vector ensemble method to the O3 dataset from the LIGO and Virgo detectors considering an ensemble of 201 known pulsars. We find no evidence for a signal from the ensemble and set a 95% credible upper limit on the mean ellipticity assuming a common exponential distribution for the pulsars' ellipticities. Using two independent hierarchical Bayesian procedures, we find upper limits of 1.2×10^{-9} and 2.5×10^{-9} on the mean ellipticity for the 201 analyzed pulsars.

I. INTRODUCTION

Continuous gravitational waves (CWs) signals are promising targets for the LIGO [1] and Virgo [2] detectors defined by persistence and near-monochromaticity over long time-scales. Among the most plausible sources of this type of signal there are spinning neutron stars with a nonaxisymmetric mass distribution [3] due to deformations from shear strains in the crust, or from magnetic stresses [4].

The signal strain amplitude depends on the ellipticity, the physical parameter that quantifies the mass distribution asymmetry with respect to the rotation axis [5]. Different neutron star equations of state can allow different sizes of deformations, i.e., of ellipticities, to be sustained in the star. The detection of a CW signal could allow us to make physical inference about the equation of state, and/or about the internal magnetic field strength [6].

According to the knowledge of the source parameters (sky position, rotation parameters), different strategies can

*ldonofrio@roma1.infn.it

be adopted to search for a CW signal [7]. The simplest, but also the most sensitive strategy, is the targeted search [8]; using information about the spin evolution, astrometry, and binary orbit gained from continued pulsar monitoring, it is possible to infer with high accuracy the sky position and the rotation parameters including the source spin frequency and the spin-down. Indeed, most pulsars are observed to steadily spin-down due to the emission of electromagnetic waves (and, possibly, also CWs). From the pulsar spin-down, it is possible to set a theoretical upper limit to the strain amplitude, the so-called spin-down limit, assuming that all of the rotation energy lost by the pulsar is converted to gravitational wave (GW) energy [9].

At the source reference frame, the CW signal is almost monochromatic with frequency proportional to the rotation frequency of the source, through a factor which depends on the considered emission model [4]. At the detector, the CW signal has a frequency and phase modulation mainly due to the Doppler effect for the relative motion between the source and the Earth.

Demodulation techniques are useful for removing the phase modulation caused by the spin-down/Doppler shift and hence to precisely unwind the apparent phase evolution of the source. Once these corrections have been applied, a CW signal would become monochromatic except for the sidereal modulation due to the antenna patterns. This modulation depends on the detector position and orientation on the Earth and it is used by the $5n$-vector method to define a detection statistic as well as to estimate the signal parameters [10,11].

So far, no evidence for a CW signal has been found in LIGO and Virgo data. The last targeted search from the LIGO-Virgo-Kagra (LVK) Collaboration [9], using the data from the observing run O3 and analyzing 236 known pulsars, set 95% credible upper limits on the amplitude and the ellipticity of each pulsar.

To improve the detection probability for the targeted search of CWs, different strategies can be used considering an ensemble of individually undetectable pulsars as in [12–14]. In this paper, we use the $5n$-vector ensemble method, described in [15]. This method defines an ensemble statistic, $T(k)$, as the partial sum of the statistics of a single pulsar, ranked for increasing p-values.

The ensemble procedure is a rank truncation method that selects the top ranking sources according to the significance of the corresponding individual test. Using the statistics $T(k)$, we define a p-value as a function of k, that is a p-value for the overall hypothesis of the presence of CWs from the ensemble.

In case of no detection, we can set 95% credible upper limit on the global parameter Λ (defined in [15]) that describes the ensemble, and on the mean ellipticity that returns information about the population properties using two independent hierarchical procedures.

The paper is organized as follows. In Sec. II, we review the $5n$-vector ensemble method and describe the procedures to set upper limits in case of no detection from the ensemble. In Sec. III, we describe the dataset used for the analysis while in Sec. IV, we show the results of the targeted search for a single pulsar using the $5n$-vector method with the first application to pulsars in binary system. In Sec. V, we report the results of the ensemble procedure on three different sets. Since there is no evidence of a signal from the ensemble, we set the upper limits, that are compared with the results of previous similar searches. Conclusions are presented in Sec. VI.

II. THE $5n$-VECTOR ENSEMBLE METHOD

The $5n$-vector ensemble method [15] is a multiple test that combines the effects of individually undetectable pulsars using the results of the single-pulsar analysis through the $5n$-vector method.

The $5n$-vector method [11] is a frequentist pipeline used in the LVK Collaboration for CW searches. It is based on the splitting at the detector of the expected GW frequency f_{gw} in five components due to the sidereal modulation of the Earth. The expected signal $h(t)$ can be written using the polarization ellipse [10],

$$h(t) = H_0\big(H_+A_+(t) + H_\times A_\times(t)\big)e^{i\Phi(t)}, \quad (1)$$

where $H_{+/\times}$ are the polarization functions for the plus and cross components:

$$H_+ = \frac{\cos(2\psi) - j\eta\sin(2\psi)}{\sqrt{1+\eta^2}}, \quad (2)$$

$$H_\times = \frac{\sin(2\psi) + j\eta\cos(2\psi)}{\sqrt{1+\eta^2}}. \quad (3)$$

η and ψ are the polarization parameters [10], $A_{+/\times}$ are linked to the antenna patterns while $\Phi(t)$ is the GW phase. The parameter η is defined as

$$\eta = -\frac{2\cos(\iota)}{1+\cos^2(\iota)}, \quad (4)$$

where ι is the angle between the star rotation axis and the line of sight. The amplitude H_0 is linked to the classic amplitude h_0, defined for example in [9], by:

$$H_0 = h_0\sqrt{\frac{1 + 6\cos^2(\iota) + \cos^4(\iota)}{4}}. \quad (5)$$

The phase $\Phi(t)$ in Eq. (1) shows a time dependence due to different phenomena that modulate in time the received signal frequency. Heterodine corrections [16] are applied to account for the pulsar spin-down and Doppler effect due to

the Earth motion. The residual modulation is in the functions $A_{+/\times}$, i.e., in the detector response, that depend on the five frequencies $f_{\text{gw}}, f_{\text{gw}} \pm \Omega_\oplus, f_{\text{gw}} \pm 2\Omega_\oplus$, where $\Omega_\oplus$ is the Earth's sidereal angular frequency.

The data 5-vector $\mathbf{X}$ and the signal template 5-vectors $\mathbf{A}^{+/\times}$ are defined as the Fourier transforms of the data and of the template functions $A_{+/\times}$ at the 5 frequencies where the signal power is split. The data/template 5-vectors from each of the n considered detectors are then combined as described in Appendix A for a multidetector analysis.

The $5n$-vector defines two matched filters between the data $\mathbf{X}$ and the signal templates $\mathbf{A}^{+/\times}$ vectors, used in order to maximize the signal-to-noise ratio,

$$\hat{H}_+ = \frac{\mathbf{X} \cdot \mathbf{A}^+}{|\mathbf{A}^+|^2} \quad \text{and} \quad \hat{H}_\times = \frac{\mathbf{X} \cdot \mathbf{A}^\times}{|\mathbf{A}^\times|^2}. \tag{6}$$

The two matched filters are estimators [10] of the signal plus and cross amplitudes. They are used to construct the detection statistic S,

$$S = \frac{|\mathbf{A}^+|^4}{\sum_{j=1}^n \sigma_j^2 T_j |\mathbf{A}_j^+|^2} |\hat{H}_+|^2 + \frac{|\mathbf{A}^\times|^4}{\sum_{k=1}^n \sigma_k^2 T_k |\mathbf{A}_k^\times|^2} |\hat{H}_\times|^2, \tag{7}$$

where σ_j^2 and T_j are the variance of the data distribution in a frequency band around f_{gw} (usually few tenths of Hz wide) and the observation time [17] in the jth detector, respectively. In the case of Gaussian noise, the distribution of the statistic S in Eq. (7) is a gamma distribution $\Gamma(x; 2, 1)$.

Fixing the number N of analyzed pulsars, the $5n$-vector ensemble method ranks these pulsars according to the p-values P_i (with $i = 1, \ldots, N$),

$$P_i = P(S_i \geq \bar{S}_i | \text{noise}) \tag{8}$$

computed from the S_i noise distribution and the measured value $\bar{S}_i$ for the ith pulsar. Then, the ensemble statistic $T(k)$ is defined as the partial sum of the first k largest-order statistics (statistics with the k smallest p-values),

$$T(k) = \sum_{j=N-k+1}^N S_{(j)}. \tag{9}$$

From the statistics $T(k)$, we can compute the p-value of ensemble $P(k)$ as a function of k,

$$P(k) = P(T(k) \geq \bar{T}(k) | \text{noise}) \tag{10}$$

with

$$\bar{T}(k) = \sum_{j=N-k+1}^N \bar{S}_{(j)}, \tag{11}$$

and $\bar{S}_{(j)}$ is the jth largest measured value for the detection statistic for a certain pulsar in the ensemble. For example, for an ensemble of N pulsars with $P_j \leq P_i \; \forall i$ and $P_k \geq P_i \; \forall i$, the smallest and the largest order statistics values are $\bar{S}_{(1)} \equiv \bar{S}_k$ and $\bar{S}_{(N)} \equiv \bar{S}_j$, respectively.

We note that the p-value refers only to the null hypothesis and does not make reference to or allow conclusions about any other hypotheses, such as the alternative hypothesis. A small p-value (for example, below the 1%) can be used to recognize interesting ensemble of pulsars as starting point for the detection.

The noise and the signal distribution of the statistics $T(k)$ can be inferred using a Monte Carlo procedure starting from the N experimental noise and signal distributions for the statistics of the single pulsar, as described in [15].

The $T(N)$ statistic coincides with the simple sum of the statistics S_i; in the case of Gaussian noise, $T(N)$ follows a $\Gamma(x; 2N, 1)$ distribution. The $T(N)$ signal distribution can be also expressed in closed form and it is proportional to a noncentral χ^2 distribution with $4N$ degrees of freedom and noncentrality parameter Λ [15],

$$\Lambda = \sum_{i=1}^N H_{0,i}^2 f_i(\eta_i, \psi_i), \tag{12}$$

where the coefficient f_i is

$$f_i(\psi_i, \eta_i) = 2\left(\frac{|\mathbf{A}_i^+|^4 |H_{+,i}|^2}{\sum_{j=1}^n \sigma_j^2 T_j |\mathbf{A}_{j,i}^+|^2} + \frac{|\mathbf{A}_i^\times|^4 |H_{\times,i}|^2}{\sum_{k=1}^n \sigma_k^2 T_k |\mathbf{A}_{k,i}^\times|^2} \right). \tag{13}$$

Even though we have defined a p-value of ensemble as a function of k, the statistical inference concerns the entire set of considered pulsars. The claim of a rank truncation method is the same of the Fisher's combination method where all the individual tests are combined together: i.e., there are some signals among all the N tests, regardless that a certain $k < N$ led to a rejection.

A. Upper-limit procedures

For the single-pulsar analysis, we can set the 95% credible upper limits on the amplitude assuming uninformative uniform priors on ψ (with $-\pi/2 \leq \psi \leq \pi/2$) and $\cos(\iota)$ [with $-1 \leq \cos(\iota) \leq 1$] that defines η [see Eq. (4)]. Knowing the distance and assuming a fiducial moment of inertia, we set the 95% credible upper limits on the ellipticity.

The upper limit for the ensemble procedure must be set on population parameters since using a multiple test, we can not infer statistical information about the single-pulsar parameters.

Considering the statistic $T(N)$, i.e., the entire set of considered pulsars, two different approaches can be used.

First, we can constrain the parameter Λ, defined in Eq. (12), that fixes the $T(N)$ distribution considering a mixed Bayesian-frequentist approach as in the case of a single pulsar [18].

For the Bayes' theorem, the posterior on Λ is

$$P\big(\Lambda|\bar{T}(N)\big) \propto L\big(\bar{T}(N)|\Lambda\big)\Pi(\Lambda), \qquad (14)$$

where $\bar{T}(N)$ is the measured value of the ensemble statistic, $\Pi(\Lambda)$ is the prior while $L(\bar{T}(N)|\Lambda)$ is the likelihood, that is estimated from the theoretical $T(N)$ signal distribution evaluated at the value $\bar{T}(N)$ for different Λ values.

The upper limit $\Lambda^{95\%}$ on the parameter Λ is

$$\Lambda^{95\%}: \quad \int_0^{\Lambda^{95\%}} P\big(\Lambda|\bar{T}(N)\big)d\Lambda = 0.95. \qquad (15)$$

Λ is a global parameter for the ensemble and $\Lambda^{95\%}$ can be used to show the improvement in the method sensitivity analyzing future runs.

Secondly, assuming a common distribution for the ellipticities, we can use a hierarchical Bayesian framework to constrain the value of the hyperparameter that fixes the assumed common distribution. Indeed, hierarchical Bayesian inference allows to study population properties for the analyzed ensemble of pulsars [19].

Let us consider an ensemble of N pulsars and a common distribution fixed by the hyperparameter μ_ϵ for the set of ellipticities ϵ_i (with $i = 1, ..., N$).

We can constrain the value of the hyperparameter μ_ϵ considering the posterior probability density function inferred from a Bayesian procedure,

$$P\big(\mu_\epsilon|\bar{T}(N)\big) \propto L\big(\bar{T}(N)|\mu_\epsilon\big)\Pi(\mu_\epsilon), \qquad (16)$$

where $\Pi(\mu_\epsilon)$ is the prior distribution on the hyperparameter, while the likelihood $L(\bar{T}(N)|\mu_\epsilon)$ can be defined as the value of the $T(N)$ signal distribution evaluated at $\bar{T}(N)$, if the common distribution of the ellipticities is fixed by the hyperparameter μ_ϵ. The $T(N)$ signal distribution and hence, the likelihood, is fixed by Λ in case of Gaussian noise. It follows that:

$$L\big(\bar{T}(N)|\mu_\epsilon\big) = \int L\big(\bar{T}(N)|\Lambda\big)\Pi(\Lambda|\mu_\epsilon)d\Lambda. \qquad (17)$$

From the definition in Eq. (12), deducing the analytical prior on Λ for an assumed distribution of the ellipticities with hyperparameter μ_ϵ is not straightforward. For a large ensemble, $N \gg 1$, $\Pi(\Lambda|\mu_\epsilon)$ can be approximated with a Gaussian distribution according to the central limit theorem. The mean and variance of the Gaussian distribution depend on the assumed distribution since it is the weighted sum of the mean and variance for the squared ϵ_i random variables.

The upper limit $\mu^{(\Lambda)}$ is

$$\mu^{(\Lambda)}: \quad \int_0^{\mu^{(\Lambda)}} P\big(\mu_\epsilon|\bar{T}(N)\big)d\mu_\epsilon = 0.95. \qquad (18)$$

Differently, we can also consider a classic hierarchical procedure combining the results of the single-pulsar analysis as in [12]. In this case, the posterior probability density function on the hyperparameter μ_ϵ is

$$P\big(\mu_\epsilon|\bar{S}_1, ..., \bar{S}_N\big) \propto \left(\prod_{i=1}^N \int L(\bar{S}_i|\epsilon_i)\Pi(\epsilon_i|\mu_\epsilon)d\epsilon_i\right)\Pi(\mu_\epsilon). \qquad (19)$$

This posterior is independent of the ensemble procedure [i.e., of the statistic $T(N)$] and depends on the results of the single-pulsar analysis through the likelihoods $L(\bar{S}_i|\epsilon_i)$. In addition, it does not depend on the Gaussian noise hypothesis and it can be used to constrain the hyperparameter μ_ϵ using the likelihood $L(\bar{S}_i|\epsilon_i)$ computed for the ith pulsar analysis. The upper limit $\mu^{(S)}$ is

$$\mu^{(S)}: \quad \int_0^{\mu^{(S)}} P\big(\mu_\epsilon|\bar{S}_1, ..., \bar{S}_N\big)d\mu_\epsilon = 0.95. \qquad (20)$$

III. DATASET

In this section, we describe the dataset used for the analysis. It consists of the GW dataset from the LIGO and Virgo detectors, and the electromagnetic dataset from the different observatories used to determine the pulsar ephemerides.

A. Gravitational wave data

The O3 observing run started on April 1, 2019 (58574.625) and ended on March 27, 2020 (58935.708) for both the LIGO and Virgo detectors. O3 consisted of two parts, separated by a one month long commissioning break. O3a ran from April 1, 2019, 15:00 UTC until October 1, 2019, 15:00 UTC. O3b ran from November 1, 2019, 15:00 UTC, to March 27, 2020, 17:00 UTC.

The duty cycles for this run were 76%, 71%, and 76% for LIGO Livingston (LLO), LIGO Hanford (LHO), and Virgo, respectively. The O3 dataset is publicly available via the Gravitational Wave Open Science Center [20].

In this paper, we use the band sampled data (BSD) framework [16] that consists of bandlimited, downsampled time series of the detector calibrated data, called BSD files. This framework can be described as a database of sub-databases where the BSD file is a complex time series that covers 10 Hz and spans 1 month of the original data. Using the BSD libraries, it is possible to extract frequency

sub-bands or time subperiods in a flexible way, reducing the computational cost of the analysis.

B. Electromagnetic data

The set of analyzed pulsars is in Table II. We consider the ephemerides used in [9].

The observatories which have contributed to the dataset [21] are the Canadian Hydrogen Intensity Mapping Experiment (CHIME) [22], the Mount Pleasant Observatory 26 m telescope, the 42 ft telescope and Lovell telescope at Jodrell Bank, MeerKAT [23], the Nançay Decimetric Radio Telescope, the Neutron Star Interior Composition Explorer (NICER) and the Molonglo Observatory Synthesis Telescope (as part of the UTMOST pulsar timing program) [24,25]. Pulsar-timing solutions were determined from this data using TEMPO [26] or TEMPO2 [27–29] to fit the model parameters. The ephemerides have been created using pulse time-of-arrival observations that mainly overlapped with O3 observing period.

To estimate the theoretical spin-down limit or the upper limit for the fiducial ellipticity for a certain source, the pulsars' distances are needed [9]. For many pulsars, the distance can be found in the ATNF Pulsar Catalog [30]. These are distances mostly based on the observed dispersion measure and estimated using the Galactic electron density distribution model YMW16 [31] or the NE2001 model [32], although others are based on parallax measurements, or inferred from associations with other objects or flux measurements.

The distances used for each pulsar are given in Table II. The distances based on the dispersion measure are estimates with uncertainties that can amount up to a factor of two [31]. Nearby pulsars, for which parallax measurements are possible, have smaller distance uncertainties.

We select pulsars whose rotation frequency is greater than 10 Hz to match the sensitivity band of the GW detectors. This leads to primarily targeting millisecond pulsars and fast spinning young pulsars. In the analyzed set, there are 165 millisecond pulsars with expected CW frequencies above 100 Hz.

Pulsars can experience glitches during the observation time (as for the Crab pulsar during O3 [9]), i.e., sudden, impulsive increases in their spin [33]. The general procedure for glitching pulsars is to analyze each interglitch period independently and then to sum the resulting statistics [9]. In this analysis, we have not considered glitching pulsars; a dedicated study is needed to optimize the detection probability when glitching pulsars are present in the ensemble.

IV. SINGLE-PULSAR ANALYSIS

In this section, we describe the results of the analysis of single pulsars using the $5n$-vector method. Differently from

the analysis in [9], we use the normalized single-pulsar statistic S defined in Eq. (7) using the weighted multidetector extension described in Appendix A. For the first time using the $5n$-vectors, we also consider pulsars in binary systems.

The results, reported in Table II, are obtained considering a single harmonic emission, i.e., the expected GW frequency is assumed exactly twice the rotation frequency of the source, and analyzing O3 data from the two LIGO and Virgo detectors.

For each pulsar, we consider a small frequency band (at least 0.2 Hz and at most 0.5 Hz wide) around the expected GW frequency. The frequency band extracted from the BSD files is chosen considering the spin-down of the source and in case of binary systems, considering also the Doppler effect due to the orbital motion.

Using the heterodyne correction [16], we remove the spin-down and the Doppler frequency modulation for the expected GW signal. The Doppler correction for pulsars in binary systems follows the model described in [34]. A test of the Doppler correction is described in Appendix B. We do not take into account the uncertainty estimates in the binary parameters; the possible effects of these uncertainties on the heterodyne correction is described in the analysis in Appendix C.

The experimental noise distribution is inferred considering a range of off-source frequencies as described in [11]. The measured value of the statistics is compared with the noise distribution computing the p-value. Using the BSD framework, the computational cost of the analysis is reduced to a few CPU-minutes per source per detector.

In agreement with [9], there is no evidence of a CW signal from any pulsar in O3 data. We set 95% credible upper limit on the amplitude h_0 for each pulsar.

For the $5n$-vector method since we are considering a different statistic, the results do not exactly coincide with the results in [9] but there is a very good agreement. For example, the upper limit on the amplitude for the pulsar J0711-6830 in [9] is 5.0×10^{-27}, while 4.8×10^{-27} in this work.

As shown in Fig. 1, the upper limits from the $5n$-vector method (red circles) are in good agreement with the results of the Bayesian method (blue stars as in [9]). The differences in the results can be due to the data frameworks that are used in the two pipelines that entail different analyzed frequency bands for each pulsar and different preprocessing of the data.

V. ENSEMBLE ANALYSIS

In this section, we show the results of the $5n$-vector ensemble method applied to O3 data. From the set of pulsars in Table II, we select 201 pulsars excluding 22 binary pulsars according to the selection criteria in Eq. (C6) described in Appendix C based on the uncertainties of the binary parameters.
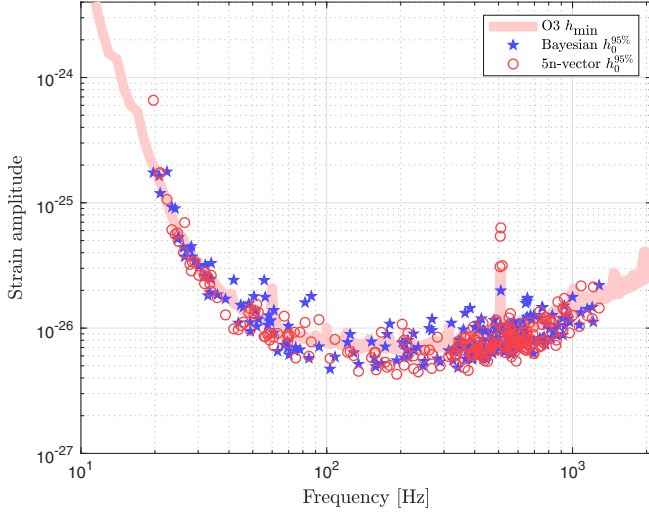
FIG. 1. Strain amplitude as a function of the GW frequency for O3 data of the LIGO and Virgo detectors. Blue stars are the upper limits inferred in [9] using the Bayesian method for the 223 pulsars in Table II while the red circles are the upper limits for the 5*n*-vector method. The continuous pink line is the minimum detectable amplitude for the O3 run considering a multidetector analysis.

As described in [15], the improvement in the detection probability for the 5*n*-vector ensemble method depends on the number of analyzed pulsars N and on the power of the combined individual tests. In a real search, we cannot optimize N since we do not know the strength of the signals *a priori*.

We fixed three different ensembles from the set in Table II; the entire set for the three detectors, the set of millisecond pulsars ($f_{\rm gw} > 100$ Hz) for the LIGO detectors and the high-value pulsars set for the LIGO detectors. High-value pulsars are the analyzed pulsars whose ratio between the experimental upper limit on the amplitude $h_0^{95\%}$ and the theoretical spin-down limit $h_{\rm sd}$ (the so-called spin-down ratio) is

$$h_0^{95\%}/h_{\rm sd} \lesssim 1. \qquad (21)$$

We chose the three ensembles according to physical observations. Indeed, millisecond pulsars are most likely to have undergone an accretion phase, which could alter the structure of their crust and magnetic field compared to nonrecycled young pulsars [35], while high-value pulsars are promising targets that have surpassed their spin-down limits.

The three ensembles correspond to fix $N = 201$ for the first set, $N = 146$ for the millisecond pulsars set and $N = 20$ for the high-value pulsars set.

After analyzing each pulsar singularly, we reconstruct the statistics $T(k)$ and compute a *p*-value of ensemble as a

function of k. The results are shown in the form of summary plot; the top-left plot shows the fitted shape and scale parameters of a gamma distribution for the experimental noise distribution for the statistic S as a function of the GW frequency, the top-right plots show the fitted shape and scale parameters to the $T(k)$ noise distributions as a function of k while the bottom-plot compares the ordered single-pulsar *p*-values (red dots) with the ensemble *p*-values from the $T(k)$ statistics (blue line).

Since there is no evidence of signal from the ensemble, we set 95% credible upper limit on the global parameter Λ and on the hyperparameter μ_e, that is the mean value of the assumed exponential distribution for the ellipticities.

A. All pulsars, all detectors

The summary plot for the entire set of analyzed pulsars is shown in Fig. 2. For this analysis, we consider the two LIGO and Virgo detectors.

A criterion based on noise is used to select the detectors for the multidetector analysis of the single pulsar. Since the normalized statistic S, in the hypothesis of Gaussian noise, is distributed according to a $\Gamma(x; 2, 1)$, from the fitted parameters to the experimental noise S distribution (top-left plot in Fig. 2) we can easily check the Gaussianity in the selected frequency band for each pulsar. For the multidetector analysis, we consider only the detectors that have fitted shape and scale parameters respectively in the range [1.6, 2.4] and [0.8, 1.2] (that is a maximum difference of 20% from the expected values for Gaussian noise). For each pulsar, this procedure allows to exclude the detectors with large noise disturbances in the analyzed frequency band. Indeed, experimental noise S distributions that are very different from the $\Gamma(x; 2, 1)$ can influence the Monte Carlo procedure for the $T(k)$ noise distributions.

From the bottom plot of Fig. 2, there is no evidence of a signal form the ensemble. One pulsar has a single-pulsar *p*-value (red dot) below 1% as expected for a set of 201 pulsars. The *p*-value computed for the statistics $T(k)$ are consistent with the noise hypothesis.

B. Millisecond pulsars, LIGO detectors

The summary plot for the millisecond pulsars is shown in Fig. 3. For this analysis, we consider only the two LIGO detectors with the same noise criteria introduced in the previous subsection, not considering the Virgo detector that has a higher noise level. As shown in Appendix A, a multidetector analysis does not necessarily entail a better sensitivity compared to the most sensitive detector's analysis.

As shown in the bottom plot in Fig. 3, there are three pulsars—J0824 + 0028, J1544 + 4937, J1551 − 0658—below the 1% threshold. There is no evidence of a signal for any of these pulsars (as for the Bayesian results in [9]);
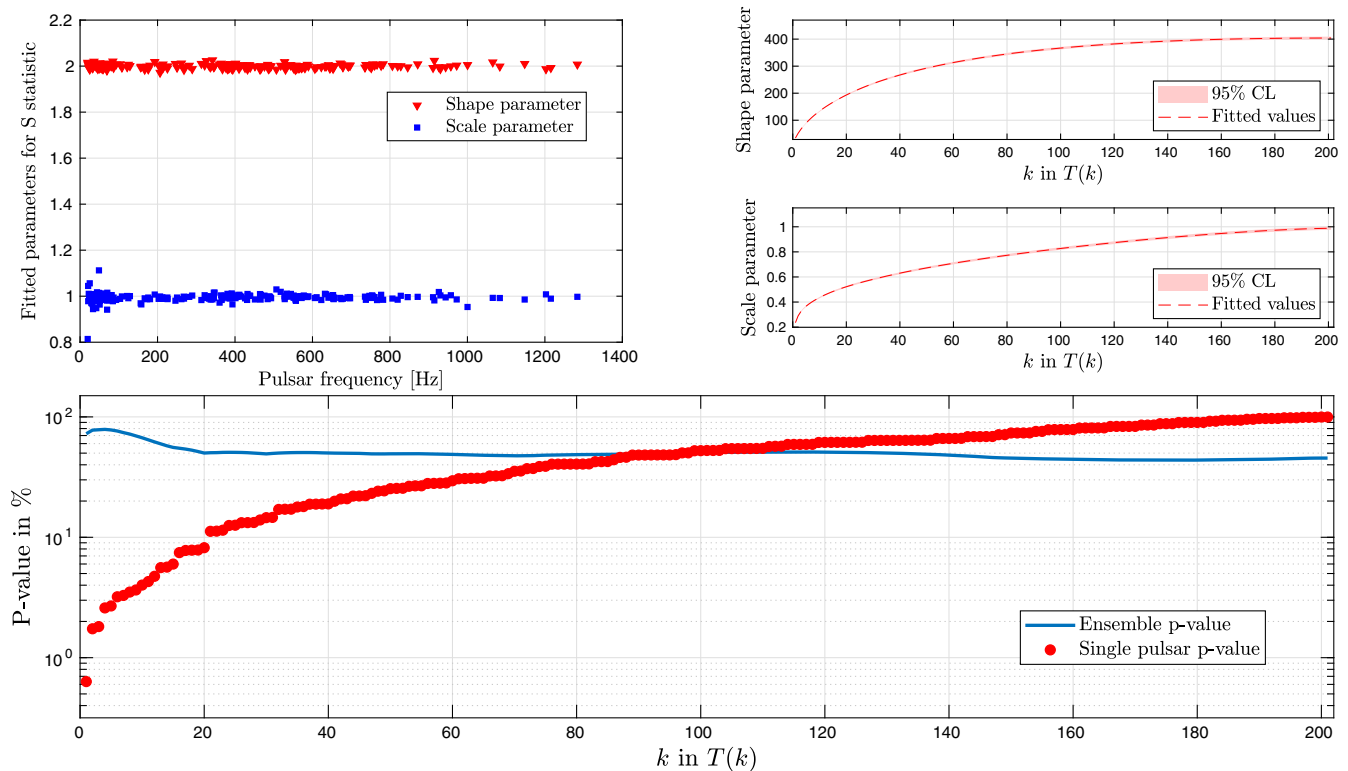
FIG. 2.   Summary plot of the results for the ensemble over 201 pulsars considering O3 data of LLO, LHO, and Virgo detectors. Top-left plot: fitted shape (red triangles) and scale parameters (blue squares) using a gamma distribution to the experimental noise distribution for each pulsar as a function of the emission frequency of the pulsar. Top-right plots: fitted shape and scale parameters (dashed lines) with 95% confidence level (colored area) for the $T(k)$ noise distributions for each k inferred from the Monte Carlo procedure. Bottom plot: p-value of ensemble (blue line) compared with the single-pulsar p-values (red dots), ranked for increasing values.

the combination of the two LIGO detectors produces lower p-values with respect to the three-detectors case.

For example considering the pulsar J0824 + 0028, the p-values for the single-detector single-pulsar analysis are 0.01, 0.04, 0.37 for LLO, LHO, and Virgo, respectively. The multidetector analysis considering all the three detectors entails a p-value of 0.01 while considering only the two LIGO detectors, the p-value is 0.002.

The ensemble p-value has a minimum of almost 3% for $k = 4$ with no evidence of a signal from the ensemble. The strong decrease for the first values of k is due to the presence of the three pulsars with p-values below 1%.

C. High-value pulsars, LIGO detectors

There are 20 high-value pulsars in our dataset, that is there are 20 pulsars with spin-down ratio $\lesssim 1$ (as in [9], excluding the glitching pulsars).

The summary plot for the high-value pulsars is shown in Fig. 4. For this analysis, we consider only the two LIGO detectors with the same noise criteria introduced in the previous subsection.

As shown by the blue line in the bottom plot of Fig. 4, the p-value of the ensemble is fully consistent with the noise hypothesis.

D. Upper limits

For the upper limit computation, we consider the set of known pulsars analyzed in Fig. 2 and the O3 dataset for the LIGO and Virgo detectors.

Using the statistic $T(N)$, that is the simple sum of the statistics for the pulsars in the analyzed ensemble, we set 95% credible upper limit on the parameter Λ defined in Eq. (12). The prior on Λ is chosen uniform while the likelihood is the value of the $T(N)$ signal distribution evaluated at the measured value $\bar{T}(N)$. The posterior $P(\Lambda|\bar{T}(N))$, shown in the left plot of Fig. 5, is compatible with zero as expected for the noise-only case. The 95% credible upper limit is

$$\Lambda^{95\%} = 84.1. \qquad (22)$$

It is not possible to infer any information for the single pulsars from the upper limit $\Lambda^{95\%}$ since Λ is a global parameter for the ensemble. $\Lambda^{95\%}$ can be used to constrain different global parameters based on some assumptions for the single-pulsar amplitudes. For example, by assuming that each pulsar in the ensemble emits a CW signal with the same amplitude $\bar{h}$, from the upper limit $\Lambda^{95\%}$ it follows that $\bar{h} = 1.9 \times 10^{-27}$.
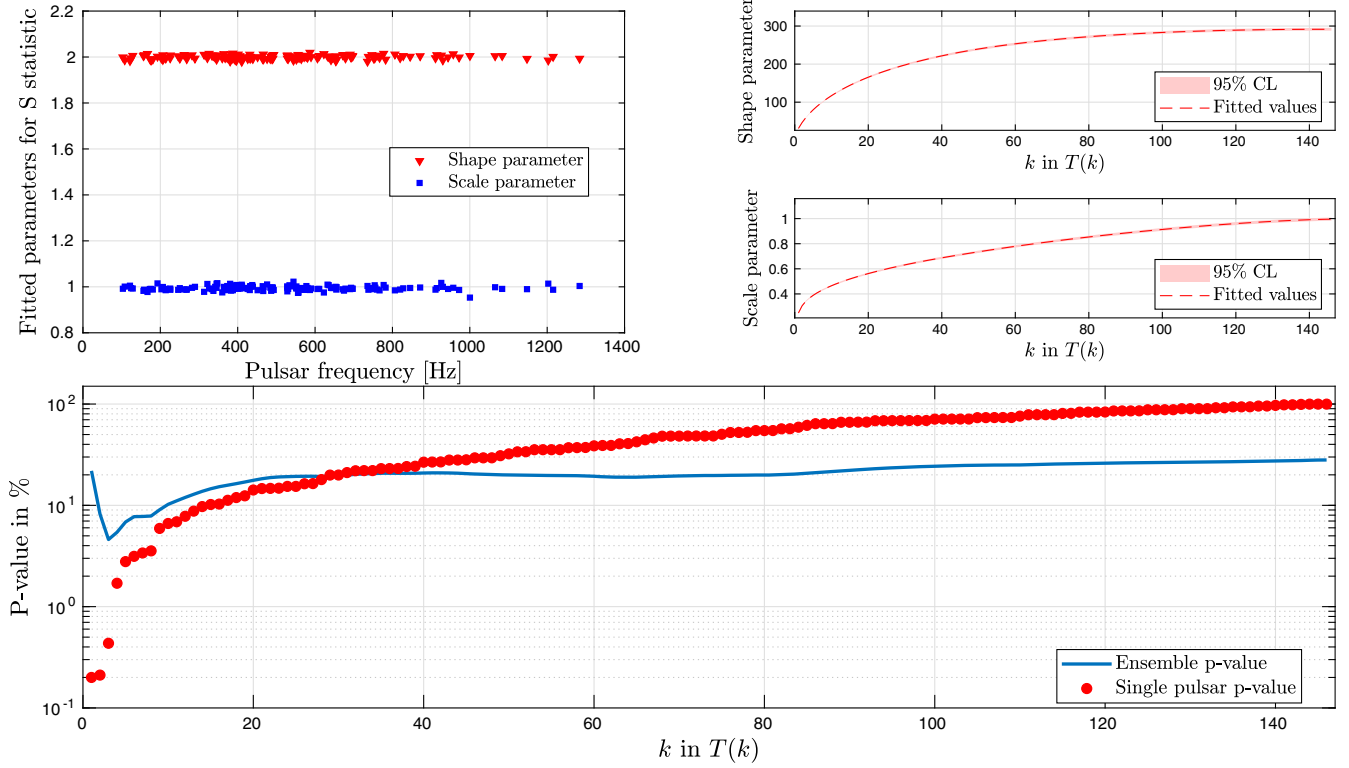
FIG. 3.   Summary plot of the ensemble composed by the millisecond pulsars in Table II, considering O3 data and the two LIGO detectors. Top-left plot: fitted shape (red triangles) and scale parameters (blue squares) using a gamma distribution to the experimental noise distribution for each pulsar as a function of the emission frequency for the considered pulsar. Top-right plots: fitted shape and scale parameters (dashed lines) with 95% confidence level (colored area) for the $T(k)$ noise distributions for each k inferred from the Monte Carlo procedure. Bottom plot: p-value of ensemble (blue line) compared with the single-pulsar p-value (red dots), ranked for increasing values.

For hierarchical procedures, following the analysis in [12] and the stochastic searches in [36,37], we assume a common exponential distribution for the ellipticities with the hyperprior $\Pi(\mu_\epsilon)$ that is log-uniform between 10^{-10} and 10^{-7}. The posteriors $P(\mu_\epsilon|\bar{T}(N))$ and $P(\mu_\epsilon|\bar{S}_1, \ldots, \bar{S}_N)$ are shown in the right plot of Fig. 5.

The upper limit $\mu_\epsilon^{(\Lambda)}$ for the hierarchical procedure using the Λ parameter is

$$\mu_\epsilon^{(\Lambda)} = 2.5 \times 10^{-9}. \tag{23}$$

This upper limit procedure considers the theoretical signal distribution to evaluate the likelihood. The theoretical distribution can be used in the hypothesis of Gaussian noise in the analyzed frequency band for each pulsar. This can be checked looking at the fitted gamma parameters for the $T(N)$ statistic in the top-right plot of Fig. 2.

The upper limit $\mu_\epsilon^{(S)}$ for the hierarchical procedure using the single-pulsar results is

$$\mu_\epsilon^{(S)} = 1.2 \times 10^{-9}. \tag{24}$$

The results and also the posteriors in Fig. 5 can be compared with Fig. 8 in [12], where the authors analyzed 92 pulsars using data from the LIGO S6 science run showing the 90% upper limit on the mean of the assumed exponential distribution of 3.8×10^{-8}.

E. Discussion

As shown in Figs. 2–4 there is no evidence for a CW signal from the three different considered ensemble. In the following, we report some comments on the results found in this work:

(1) The upper limits set in this paper on the mean of the exponential distribution for the set of analyzed pulsars are more than one order of magnitude below the value in [12]. The combined O3 data for the LIGO and Virgo detectors are largely more sensitive than the LIGO S6 science run data and the analyzed ensemble is larger. A more reliable comparison between the two pipelines should consider the same ensemble, i.e., the same pulsars, and is outside the scope of this paper.
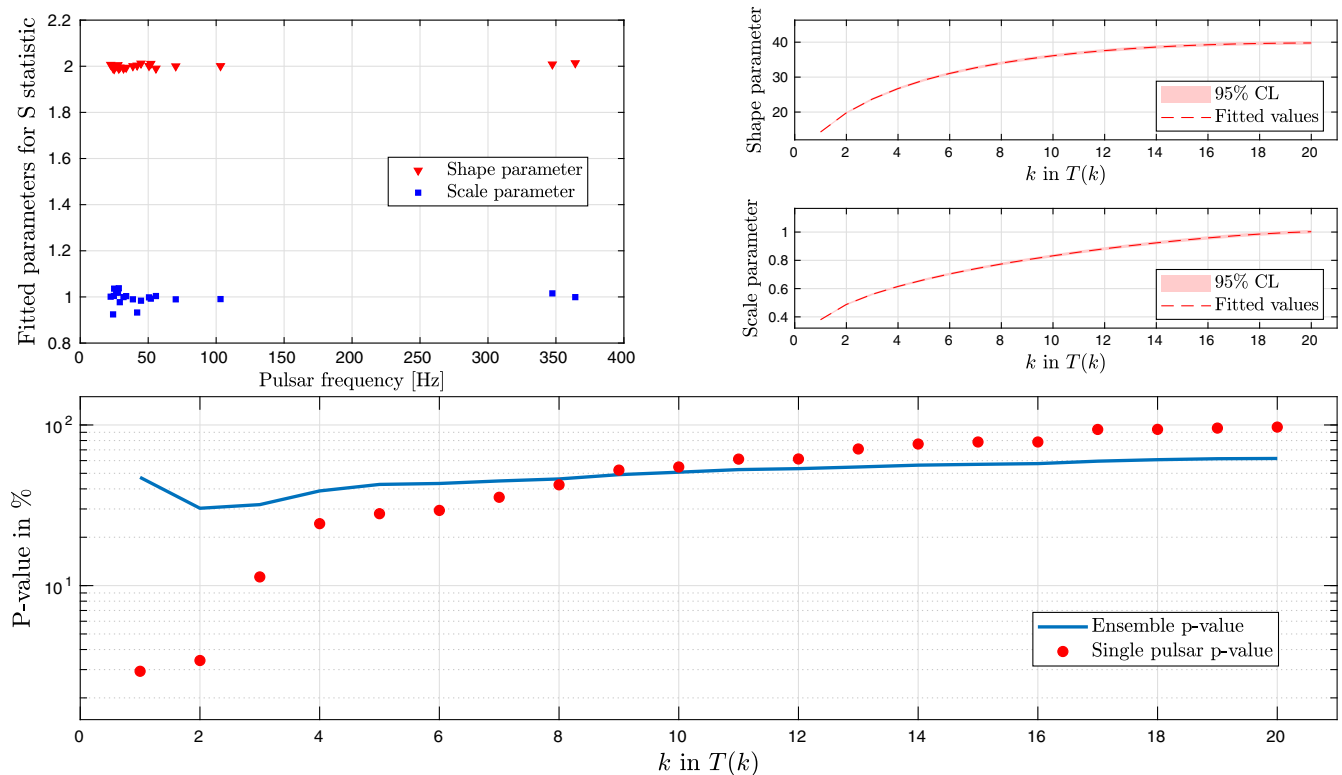
FIG. 4. Summary plot of the ensemble composed by the high-value pulsars with spin-down ratio $\lesssim 1$ considering O3 data and the two LIGO detectors. Top-left plot: fitted shape (red triangles) and scale parameters (blue squares) using a gamma distribution to the experimental noise distribution for each pulsar as a function of the frequency for the considered pulsar. Top-right plots: fitted shape and scale parameters (dashed lines) with 95% confidence level (colored area) for the $T(k)$ noise distributions for each k inferred from the Monte Carlo procedure. Bottom plot: p-value of ensemble (blue line) compared with the single-pulsar p-value (red dots), ranked for increasing values.

(2) The lowest limit on the ellipticity from the targeted search in [9] is 3.2×10^{-9} for J0636 + 5129 while from the all-sky search in [38] is 1.4×10^{-9} for a neutron star at 10 pc and 2047.5 Hz. The upper limits on the mean ellipticity set in this work are consistent with these values. We also note that these results approach the minimum limit on the ellipticity for millisecond pulsars of $\approx 10^{-9}$ supposed in [39].

(3) The upper limits in [36,37] on average ellipticity for the neutron star population are $\mathcal{O}(10^{-8})$ from cross-correlation-based searches of a stochastic gravitational wave background. These limits can not be directly compared with the limits in this work since we focused on known pulsars that represent only a small subset of the entire set of neutron stars in our Galaxy.

(4) The upper limits on the hyperparameter for the exponential distribution do not consider the uncertainties on the distance. The distance should be included as a variable assuming, for example following [12], a Gaussian prior with a mean given by each pulsar's best-fit distance, and a standard deviation of 20% of that value with a hard cutoff at zero.

(5) The hierarchical procedures assume that all the analyzed pulsar ellipticities are drawn from a common distribution that can be too simplistic to describe the true ϵ distribution. For example, the population of young pulsars and old recycled millisecond pulsars have undergone different evolution and so have a different distribution. These populations should be treated independently, or a more complex distribution that allows separation of the two distributions should be used [12]. Therefore, a bimodal distribution, or two independent exponential distributions with different mean values, could be more appropriate and worth of study.

(6) Using the multidetector procedure, the results of the single-pulsar analysis in Fig. 1 are in agreement with [9]. However, it is still not clear when a multidetector analysis outperforms the most sensitive detector analysis. To choose which detectors
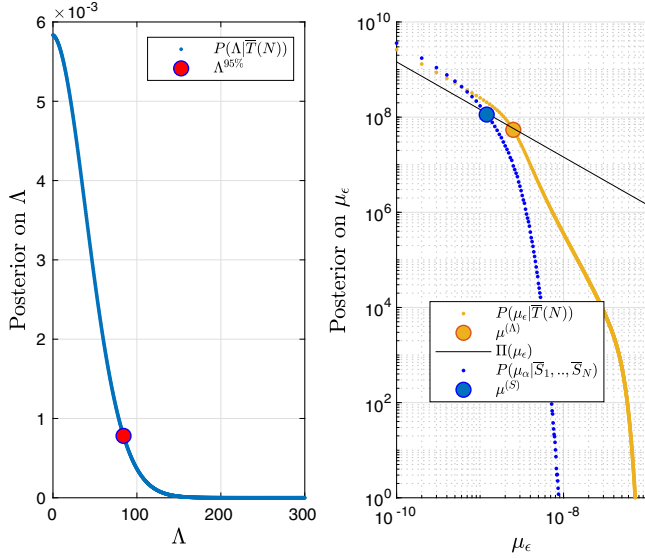
FIG. 5. Upper limits inferred from the ensemble procedure considering the set of 201 pulsars in Fig. 2 and considering the O3 data for the LIGO and Virgo detectors. Left plot: posterior distribution for the global parameter Λ [defined in Eq. (12)]. The red point indicates the 95% credible upper limit for Λ. Right plot: posterior distribution for the two independent hierarchical procedures to set the upper limits on the mean μ_ϵ of the assumed exponential distribution. The continuous line is the log-uniform hyperprior on μ_ϵ. The blue and yellow points indicate the 95% credible upper limit for μ_ϵ.

should be used in the multidetector case, criteria based on the source sky position, on the detectors' sensitivities and observation times will be studied in the next future.

VI. CONCLUSION

In this paper, we have described the application of the $5n$-vector ensemble method to O3 data for the LIGO and Virgo detectors considering a set of 201 known pulsars.

The single-pulsar analysis can be seen as an hypothesis test where the null hypothesis of pure noise is tested against the alternative hypothesis of the presence of a CW signal in the data. To improve the detection probability, we apply the $5n$-vector ensemble method, a multiple test that combines multidetector single-pulsar statistics defined through the $5n$-vector method.

For the analysis of the single pulsar, the single harmonic search (i.e., gravitational wave frequency exactly twice the rotation frequency of the source) on the 223 known pulsars shows good agreement with the Bayesian results in [9]. For the first time, the $5n$-vector method is applied to binary systems for the targeted search and compared with the Bayesian results. The dual harmonic search (GW frequency at both once and twice the rotation frequency) is not

implemented for the $5n$-vector method. In Appendix C, we describe a preliminary analysis to quantify the effect of the binary parameters uncertainties on the detection sensitivity. We exclude from the ensemble analysis 22 binary pulsars whose combined uncertainties on t_p and ω do not respect the selection criteria in Eq. (C6).

The ensemble statistics $T(k)$ for the rank truncation method is defined as the partial sum of the k largest order statistics to control the look-elsewhere effect. Reconstructing the $T(k)$ noise distributions for each k, using a Monte Carlo procedure, we compute the p-value of ensemble as a function of k, that is a p-value for the overall hypothesis of the presence of CWs from the ensemble.

In case of no detection, we propose different procedures to set upper limits using the ensemble procedure and the statistic $T(N)$, i.e., the statistic for the entire ensemble. Using a mixed frequentist-Bayesian procedure, we can constrain the value of the global parameter Λ that fixes the $T(N)$ signal distribution. Assuming a common exponential distribution for the ellipticities, we propose two independent hierarchical procedures to set an upper limit on the mean μ_ϵ of the assumed distribution.

Section V shows the application of the ensemble procedure to the set of 223 pulsars in Table II considering O3 data. Glitching pulsars, as the Crab, are not considered in the single-pulsar analysis and therefore, also in the ensemble analysis. In future searches, glitching pulsars can be included in the ensemble procedure considering the resulting statistic for the single-pulsar analysis, or considering each interglitch period as an independent pulsar.

Three different ensembles are analyzed: the full set for the LIGO and Virgo detectors, the millisecond pulsar set for the two LIGO detectors and the high-value pulsars set for the two LIGO detectors. The results are shown in the summary plots in Figs. 2–4.

There is no evidence of a CW signal from the ensemble; the p-values as a function of k are well above the assumed 1% threshold.

The upper limits procedures are applied to the entire set of pulsars considering the LIGO and Virgo detectors and O3 data. The posterior on the Λ parameter and on μ_ϵ are shown in Fig. 5. The upper limit set on Λ is $\Lambda^{95\%} = 84.1$ while the upper limit on μ_ϵ is 2.5×10^{-9} for the hierarchical procedure using the Λ parameter, and 1.2×10^{-9} for the hierarchical procedure using the single-pulsar results. These results are more than one order of magnitude below the upper limit in [12], where the authors considered a classic hierarchical Bayesian procedure on an ensemble of 92 pulsars and data from the LIGO S6 science run.

The $5n$-vector ensemble method improves the detection probability for the targeted search of CWs from known pulsars. Application of this procedure on the next observing runs will improve the possibility to detect a CW signal from known pulsars for the first time.

APPENDIX A: WEIGHTED MULTIDETECTOR EXTENSION

Considering n detectors, the classic $5n$-vector definition, described in [43], combines together the 5-vectors $\mathbf{X_i}$ from the ith detector,

$$\mathbf{X} = [\mathbf{X}_1, ..., \mathbf{X}_n]. \tag{A1}$$

Since the detectors can have different sensitivities, the statistic based on the $5n$-vector can reduce the signal to noise ratio compared to the statistic based only on the 5-vector of the most sensitive detector.

In this paper, we define the weighted data $5n$-vector as

$$\mathbf{X} = \left[c_1\mathbf{X}_1, ..., c_n\mathbf{X}_n\right], \tag{A2}$$

where the weights c_j are defined as

$$c_j = \frac{\sqrt{n}}{\sqrt{\sum_{i=1}^n \left(\frac{T_i}{S_i}\right)}}\sqrt{\frac{T_j}{S_j}} = \sqrt{\mathcal{H}}\sqrt{\frac{T_j}{S_j}}. \tag{A3}$$

S_j and T_j are the variance of the data in a small frequency band around the expected GW frequency and the observation time in the jth detector, respectively. $\mathcal{H}$ is the harmonic mean of the time-weighted variances.

The matched filter is (similarly for $\hat{H}_\times$)

$$\hat{H}_+ = \frac{\mathbf{X} \cdot \mathbf{A}^+}{|\mathbf{A}^+|^2} = \frac{\sum_{j=1}^n c_j\mathbf{X}_j(\mathbf{A}_j^+)^*}{\sum_{k=1}^n \mathbf{A}_k^+(\mathbf{A}_k^+)^*}$$
$$= \frac{1}{|\mathbf{A}^+|^2}\left(c_1|\mathbf{A}_1^+|^2\hat{H}_{+,1} + \cdots + c_n|\mathbf{A}_n^+|^2\hat{H}_{+,n}\right). \tag{A4}$$

In the hypothesis of Gaussian noise for the jth detector with variance σ_j^2, the two complex estimators $\hat{H}_{+/\times}$ also have Gaussian distributions,

$$\hat{H}_{+/\times} \sim \text{Gauss}\left(x; 0, \sigma_{+/\times}^2\right) \tag{A5}$$

with

$$\sigma_{+/\times}^2 = \sum_{j=1}^n \frac{(c_j\sigma_j)^2 T_j|\mathbf{A}_j^{+/\times}|^2}{|\mathbf{A}^{+/\times}|^4}. \tag{A6}$$

Using the c_j, we redefine the noise variance in each detector,

$$(c_j\sigma_j)^2 \propto c_j^2 S_j = \frac{nT_j}{\sum_{i=1}^n \left(\frac{T_i}{S_i}\right)}. \tag{A7}$$

If the observation time was the same ($\forall j, T_j = t$), this corresponds to "equalize" the noise in each detector.

In this case, it follows that:

$$\sigma^2_{+/\times} = \sum_{j=1}^{n} \frac{(c_j\sigma_j)^2 T_j |\mathbf{A}_j^{+/\times}|^2}{|\mathbf{A}^{+/\times}|^4} = \sum_{j=1}^{n} \frac{nt|\mathbf{A}_j^{+/\times}|^2}{\sum_{i=1}^{n}\left(\frac{1}{\sigma_i^2}\right)|\mathbf{A}^{+/\times}|^4}$$

$$= \frac{nt}{\sum_{i=1}^{n}\left(\frac{1}{\sigma_i^2}\right)|\mathbf{A}^{+/\times}|^2} = \frac{nt}{\sum_{i=1}^{n}\left(\frac{1}{\sigma_i^2}\right)\sum_{k=1}^{n}|\mathbf{A}_k^{+/\times}|^2}. \tag{A8}$$

Let us consider the toy case of n colocated detectors where $|\mathbf{A}_k^{+/\times}|^2 = |\mathbf{A}_1^{+/\times}|^2$, $\forall$ k; the variances are

$$\sigma^2_{+/\times} = \frac{t}{\sum_{i=1}^{n}\left(\frac{1}{\sigma_i^2}\right)|\mathbf{A}_1^{+/\times}|^2}. \tag{A9}$$

This corresponds to the case of one detector with observation time t and variance V^2,

$$V^2 = \frac{1}{\sum_{i=1}^{n}\left(\frac{1}{\sigma_i^2}\right)} = \frac{\mathcal{H}}{n}, \tag{A10}$$

where $\mathcal{H}$ is the harmonic mean of the variances. Since there is the condition

$$\min\{\sigma_1^2, ..., \sigma_n^2\} \le \mathcal{H} \le n\min\{\sigma_1^2, ..., \sigma_n^2\}, \tag{A11}$$

this means that

$$\frac{\min\{\sigma_1^2, ..., \sigma_n^2\}}{n} \le \frac{\mathcal{H}}{n} \le \min\{\sigma_1^2, ..., \sigma_n^2\}. \tag{A12}$$

It follows that for n colocated detectors with the same observation time, we always have an improvement in the detection sensitivity using the coefficients c_j.

For example, let us consider the case of two colocated detectors $n = 2$ (equal to consider different datasets of the same detector), with $\sigma_2^2 = C\sigma_1^2$ and $C > 1$,

$$\sigma^2_{+/\times} = \frac{C\sigma_1^2 t}{(C+1)|\mathbf{A}_1^{+/\times}|^2}. \tag{A13}$$

The minimum detectable signal is $h_{\min}$,

$$h_{\min} \propto \sqrt{\frac{C}{C+1}\frac{\sigma_1^2}{t}}. \tag{A14}$$

It is clear that in the general case (different detectors' locations and observation times), the multidetector analysis not necessarily outperforms the most sensitive detectors.

It is important to briefly describe the signal distribution for $|\hat{H}_{+/\times}|^2$, see also [11]. If a CW signal is present into the analyzed data, the distributions of the two complex estimators $\hat{H}_{+/\times}$ are

$$\hat{H}_{+/\times} \sim \text{Gauss}\big(x; H_0 e^{j\gamma} H_{+/\times} M_{+/\times}, \sigma^2_{+/\times}\big), \tag{A15}$$

where $H_{+/\times}$ are the polarization functions, H_0 is the amplitude, γ the phase and

$$M_{+/\times} = \sum_{j=1}^{n} \frac{c_j |\mathbf{A}_j^{+/\times}|^2}{|\mathbf{A}^{+/\times}|^2} \tag{A16}$$

is a known factor for the targeted search. $|\hat{H}_{+/\times}|^2$ have a noncentral-χ^2 distribution (apart from the factor $k_{+/\times}$),

$$|\hat{H}_{+/\times}|^2 \sim \frac{k_{+/\times}}{2} e^{-\frac{k_{+/\times}x + \lambda_{+/\times}}{2}} I_0\Big(\sqrt{k_{+/\times}\lambda_{+/\times}x}\Big), \tag{A17}$$

where I_0 is the modified Bessel function of the first kind, and

$$k_{+/\times} = \frac{2}{\sigma^2_{+/\times}} \qquad \lambda_{+/\times} = k_{+/\times}|H_{+/\times}|^2 H_0^2 M_{+/\times}. \tag{A18}$$

With respect to the classic definition of the $5n$-vector, the distributions do not change. There is just a redefinition of the variances for the detectors noise. This means that using the coefficients c_j, it is changed how $\lambda_{+/\times}$ depends on the detectors' sensitivity.

APPENDIX B: TEST OF THE BINARY CORRECTION

Hardware injections are simulated signals added to the detectors data physically displacing the detectors' test masses [44]. Differential displacement of the test masses mimics the detectors' response to a GW signal. Continuous hardware injections can be used to test CW analysis methods.

During the O3 run, 17 hardware injections that simulate different CW signals from spinning neutron stars were added in the two LIGO detectors. The list of injected pulsar parameters can be found in [45].

In this section, we consider two different hardware injections to test the $5n$-vector pipeline. We report the results for the injected pulsar P03 [SNR(1 yr) $\approx$30] that simulates an isolated spinning neutron stars with $f_{\text{gw}} \simeq 108.8$ Hz and for P16 [SNR(1 yr) $\approx$68], a neutron star in binary system with $f_{\text{gw}} \simeq 234.5$ Hz. Figures 6 and 7 show the amplitude spectral density for LLO detector in the frequency band around the expected GW frequency for P03 and P16 after the Doppler and spin-down corrections using the BSD heterodyne method. The red dots are the theoretical expected five frequency peaks for the GW signal due to the sidereal modulation. The different "heights" of corresponding peaks in the two detectors depend on the antenna pattern, i.e., on the signal 5-vector templates $\mathbf{A}^{+/\times}$. It is important to note that the formalism used to construct
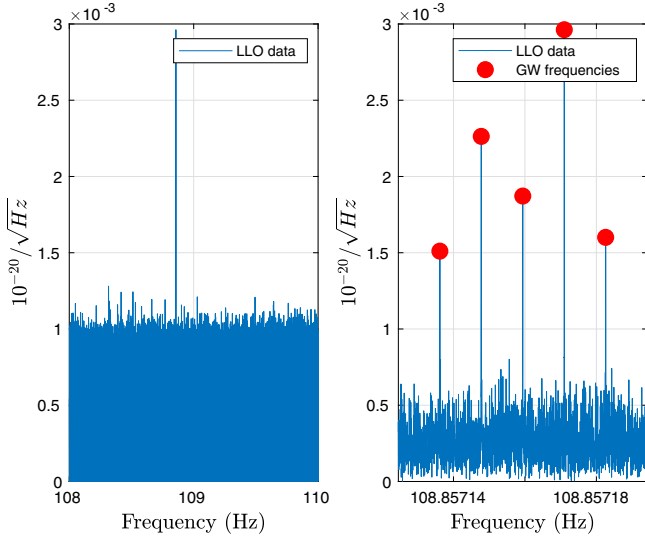
FIG. 6. Amplitude spectral density for P03 and LLO data after the corrections for Doppler and spin-down effect. The right plot is the zoom around the GW frequency; the red dots show the expected five frequencies due to the Earth sidereal motion. Central peak frequency is the expected GW frequency.
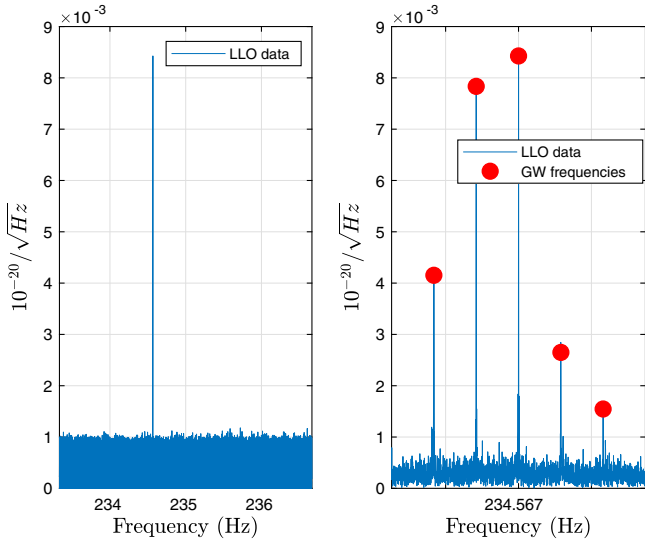

FIG. 7. Amplitude spectral density for P16 and LLO data after the corrections for Doppler and spin-down effect. The right plot is the zoom around the GW frequency; the red dots show the expected 5 frequencies due to the Earth sidereal motion. Central peak frequency is the expected GW frequency.

the hardware injections' signal is independent from the 5-vector method.

In Table I, there are the results obtained for the two hardware injections considering the O3 datasets of the two LIGO detectors. The estimation of the intrinsic parameters (see [10]) is not influenced by the choice of the detection statistic since it depends only on the estimators $\hat{H}_{+/\times}$.

TABLE I. Table of the parameters mismatch for the hardware injections (HI) P03 and P16 analyzing O3 data from the two LIGO detectors. ϵ_{H_0} is the ratio between the estimated and injected amplitude, while ϵ_η and ϵ_ψ are the normalized relative errors for the polarization parameters.

HI	Detector	ϵ_{H_0}	ϵ_η (%)	ϵ_ψ (%)
P03	LLO	0.93	0.54	1.49
	LHO	0.95	1.27	0.39
P16	LLO	0.91	0.66	$\cdots$
	LHO	0.93	0.90	$\cdots$

The small discrepancies (below 10%) in Table I for the amplitude fall within the uncertainties of the actuation system used for the injections. For P16, the ψ parameter is not well-defined, since $\eta \approx 1$ and the signal is nearly circularly polarized.

APPENDIX C: ORBITAL PARAMETERS UNCERTAINTIES

In this appendix, we describe a preliminary analysis on the possible effects of the uncertainties on the heterodyne demodulation correction in the 5-vector context. We also describe the selection criteria used in this paper to include pulsars in binary systems for the ensemble procedure. Indeed, large orbital parameters uncertainties could affect the sensitivity of targeted searches since large mismatches on the binary parameters could reduce the signal-to-noise ratio. The heterodine correction is applied by multiplying the data by the exponential factor $e^{-i\Phi_{\mathrm{corr}}(t)}$. The total signal phase correction $\Phi_{\mathrm{corr}}(t)$ can be written as the sum of the spin-down and the Doppler contribution. The Doppler contribution is the sum of the terms due to the Earth motion and due to the pulsar orbital motion $\Phi_{\mathrm{bin}}(t)$. For the linear-phase model and the small-eccentricity limit, $e \ll 1$ (details in [34]),

$$\Phi_{\mathrm{bin}}(t) \approx 2\pi f\left[-a_p\left(\sin\psi(t) + \frac{k}{2}\sin 2\psi(t) - \frac{\beta}{2}\cos 2\psi(t)\right)\right],$$
$$(C1)$$

where a_p is the semimajor axis while k and β are the Laplace-Lagrange parameters,

$$k \equiv e\cos(\omega), \qquad \beta \equiv e\sin(\omega). \qquad (C2)$$

The mean orbital phase is

$$\psi(t) = \Omega(t - t_{\mathrm{asc}}) \qquad (C3)$$

measured from the time of ascending nodes t_{asc}. For small eccentricity and mean-orbital angular velocity $\Omega = \frac{2\pi}{P}$ (P is the orbital period), t_{asc} is
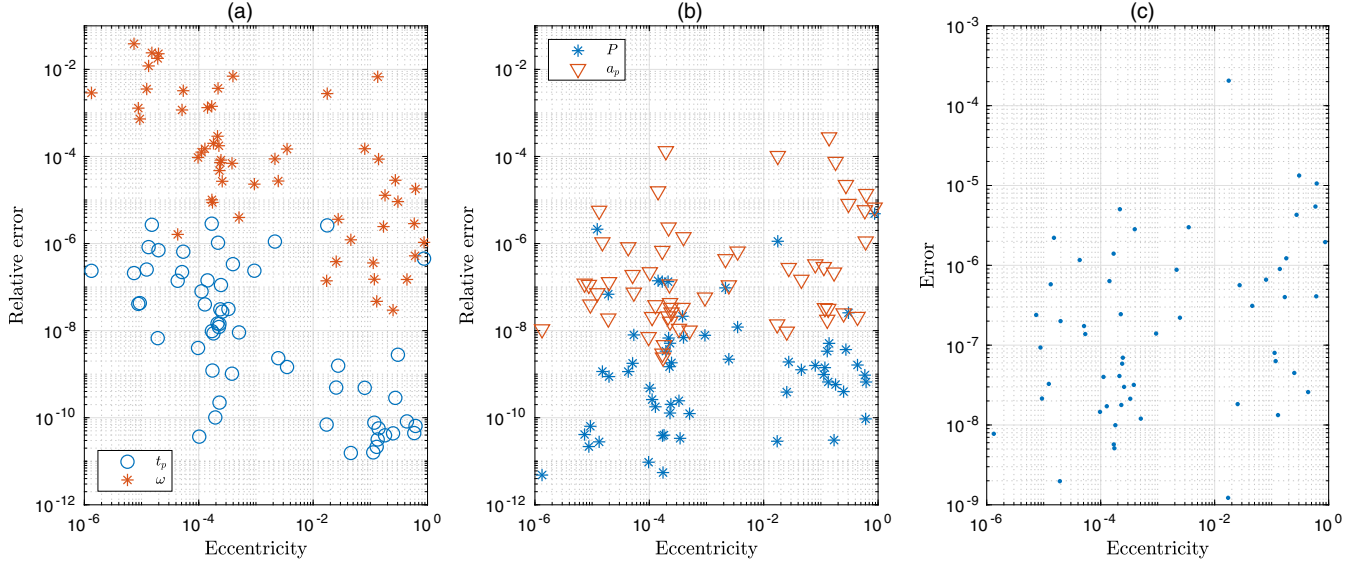
FIG. 8. Uncertainties for the orbital parameters provided by the T2 model. (a) Relative errors on t_p and ω as a function of the eccentricity. (b) Relative errors on P and a_p as a function of the eccentricity. (c) 1-σ errors on the eccentricity as a function of the eccentricity values.

$$t_{\rm asc} = t_p - \frac{\omega}{\Omega}, \tag{C4}$$

where t_p and ω are the time and the argument of periapse, respectively. There are two main models for the orbital parameters [29]: the T2 model that returns the parameters (P, a_p, t_p, ω, e) and the ELL1 model that returns the parameters $(P, a_p, t_{\rm asc}, k, \beta)$. Indeed in the low-eccentricity limit, the T2 model returns highly correlated values for t_p and ω, and the ELL1 model was developed for pulsars in such orbits.

In our preliminary analysis on the effects of the uncertainties, we focus on the T2 model since the ELL1 model provides better constrained parameters. For the ensemble of pulsars considered in our manuscript, almost 80 pulsars follows the T2 model. The parameters with the larger relative uncertainties are t_p and ω as shown in Fig. 8 (particularly when the orbital eccentricity is below 0.01 as expected). These two parameters are also expected to be more relevant since they contribute directly to the orbital phase $\psi(t)$. We note that for 15 pulsars from the T2 model, we do not have an estimation of Δt_p while 11 pulsars are in circular orbits with $e = \omega = 0$.

Using the P16, we have computed the coherence [46] for a wide range of the uncertainties Δt_p and $\Delta\omega$. The results show minima in the coherence corresponding to certain values of the combination,

$$\Delta\psi = \Omega\Delta t_p + \Delta\omega. \tag{C5}$$

The values of $\Delta\psi$ corresponding to the minima can be analytically computed from the phase $\Phi_{\rm bin}$ considering a mismatch Δt_p and $\Delta\omega$.

We fix a threshold using the value of $\Delta\psi$ associated to the first minimum,

$$\Delta\psi \sim F \cdot \frac{3}{8fa_p}. \tag{C6}$$

We can take the factor $F = 5$, which seems reasonable considering that the first minima are very sharp. Considering the 223 pulsars analyzed in Table II, 80 pulsars have parameters form the T2 model; 22 pulsars (J0218 + 4232, J1017 − 7156, J1125 − 5825, J1312 + 0051, J1529 − 3828, J1545 − 4550, J1603 − 7202, J1614 − 2230, J1630 + 3734, J1708 − 3506, J1709 + 2313, J1737 − 0811, J1750 − 2536, J1751 − 2857, J1835 − 0114, J1840 − 0643, J1904 + 0412, J1946 + 3417, J1949 + 3106, J2019 + 2425, J2053 + 4650, J2129 − 5721) have a $\Delta\psi$ above the threshold in Eq. (C6). We have excluded these pulsars from the ensemble analysis.

We stress that the uncertainties provided by the binary model are 1σ Gaussian errors while in our relation, Δt_p and $\Delta\omega$ are considered as an absolute error.

The preliminary results described in this response consider only the t_p and ω parameters; it remains unclear how the uncertainties of the entire set of parameters combine together in the heterodyne correction. A precise and independent analysis is still required and falls beyond the scope of our paper.

TABLE II.   Table of the parameters (name, GW frequency in Hz, distance in kpc, spin-down limit h_{sd}) and the results inferred using the 5n-vector method (upper limit on the amplitude $h_0^{95\%}$, upper limit on the ellipticity $\epsilon^{95\%}$, p-value) for the 223 analyzed pulsars. Some pulsars do not have a value for h_{sd}, and $\epsilon^{95\%}$ since the corresponding distance value (or the frequency derivative value) is not available in the ATNF Catalog [30]. More details about the references for the ephemerides and distance estimation for the analyzed pulsars are in [9].

Pulsar name (J2000)	f_{gw} (Hz)	Distance (kpc)	h_{sd}	$h_0^{95\%}$	$\epsilon^{95\%}$	P-value
J0023 + 0923	655.7	1.1	1.3×10^{-27}	8.2×10^{-27}	2.0×10^{-8}	0.68
J0030 + 0451	411.1	0.3	3.6×10^{-27}	6.5×10^{-27}	1.2×10^{-8}	0.71
J0034 − 0534	1065.4	1.4	8.9×10^{-28}	1.0×10^{-26}	1.2×10^{-8}	0.93
J0101 − 6422	777.3	1.0	9.7×10^{-28}	1.2×10^{-26}	1.9×10^{-8}	0.11
J0102 + 4839	674.7	2.3	6.8×10^{-28}	7.3×10^{-27}	3.5×10^{-8}	0.81
J0117 + 5914	19.7	1.8	1.1×10^{-25}	6.6×10^{-25}	2.8×10^{-3}	0.66
J0125 − 2327	544.2	0.9	2.0×10^{-27}	8.1×10^{-27}	2.4×10^{-8}	0.48
J0154 + 1833	845.8	1.6	3.4×10^{-28}	1.1×10^{-26}	2.5×10^{-8}	0.4
J0218 + 4232	860.9	3.1	1.5×10^{-27}	8.0×10^{-27}	3.2×10^{-8}	1
J0340 + 4130	606.2	1.6	7.2×10^{-28}	9.1×10^{-27}	3.7×10^{-8}	0.33
J0348 + 0432	51.1	2.1	9.3×10^{-28}	1.4×10^{-26}	1.0×10^{-5}	0.2
J0406 + 3039	766.7	$\cdots$	$\cdots$	8.0×10^{-27}	$\cdots$	0.85
J0407 + 1607	77.8	1.3	1.1×10^{-27}	9.3×10^{-27}	1.9×10^{-6}	0.2
J0437 − 4715	347.4	0.2	8.0×10^{-27}	7.4×10^{-27}	9.3×10^{-9}	0.24
J0453 + 1559	43.7	0.5	3.1×10^{-27}	9.7×10^{-27}	2.5×10^{-6}	1
J0509 + 0856	493.1	0.8	9.6×10^{-28}	6.7×10^{-27}	2.1×10^{-8}	0.83
J0509 + 3801	26.1	1.6	5.3×10^{-27}	4.0×10^{-26}	8.7×10^{-5}	0.7
J0557 + 1550	782.4	1.8	7.5×10^{-28}	1.1×10^{-26}	3.2×10^{-8}	0.33
J0557 − 2948	45.8	4.3	2.4×10^{-28}	1.1×10^{-26}	2.1×10^{-5}	0.65
J0609 + 2130	35.9	0.6	2.9×10^{-27}	1.8×10^{-26}	7.3×10^{-6}	0.73
J0610 − 2100	518.0	3.3	1.3×10^{-28}	3.2×10^{-26}	3.6×10^{-7}	0.63
J0613 − 0200	653.2	0.6	2.2×10^{-27}	6.9×10^{-27}	9.2×10^{-9}	0.96
J0614 − 3329	635.2	0.6	3.0×10^{-27}	8.2×10^{-27}	1.2×10^{-8}	0.56
J0621 + 1002	69.3	0.4	2.4×10^{-27}	8.8×10^{-27}	7.3×10^{-7}	0.34
J0636 − 3044	506.9	0.7	2.6×10^{-27}	3.1×10^{-26}	8.1×10^{-8}	0.71
J0636 + 5129	697.1	0.2	4.2×10^{-27}	6.3×10^{-27}	2.6×10^{-9}	1
J0645 + 5158	225.9	1.2	3.7×10^{-28}	4.7×10^{-27}	1.1×10^{-7}	0.86
J0709 + 0458	58.1	1.2	2.2×10^{-27}	9.1×10^{-27}	3.1×10^{-6}	0.78
J0711 − 6830	364.2	0.1	1.2×10^{-26}	4.8×10^{-27}	3.8×10^{-9}	0.91
J0721 − 2038	128.7	2.7	5.1×10^{-28}	6.0×10^{-27}	9.2×10^{-7}	0.59
J0732 + 2314	489.0	1.1	8.5×10^{-28}	6.8×10^{-27}	3.1×10^{-8}	0.76
J0740 + 6620	693.1	1.1	1.1×10^{-27}	1.0×10^{-26}	2.3×10^{-8}	0.21
J0751 + 1807	574.9	0.6	1.9×10^{-27}	8.4×10^{-27}	1.4×10^{-8}	0.62
J0824 + 0028	202.8	1.7	1.8×10^{-27}	1.1×10^{-26}	4.2×10^{-7}	0.01
J0835 − 4510	22.4	0.3	3.4×10^{-24}	1.1×10^{-25}	5.6×10^{-5}	0.26
J0921 − 5202	206.6	0.4	2.9×10^{-27}	5.1×10^{-27}	4.5×10^{-8}	0.73
J0931 − 1902	431.2	3.7	1.8×10^{-28}	5.9×10^{-27}	1.1×10^{-7}	0.84
J0955 − 6150	1000.3	2.2	9.9×10^{-28}	1.3×10^{-26}	2.6×10^{-8}	0.51
J1012 − 4235	644.9	0.4	3.1×10^{-27}	7.9×10^{-27}	6.7×10^{-9}	0.61
J1012 + 5307	380.5	0.7	1.6×10^{-27}	7.2×10^{-27}	3.3×10^{-8}	0.3
J1017 − 7156	855.2	3.5	2.5×10^{-28}	7.3×10^{-27}	3.3×10^{-8}	0.97
J1022 + 1001	121.6	0.6	1.8×10^{-27}	6.4×10^{-27}	2.6×10^{-7}	0.56
J1024 − 0719	387.4	1.2	$\cdots$	6.1×10^{-27}	4.6×10^{-8}	0.75
J1035 − 6720	696.4	1.5	2.2×10^{-27}	6.5×10^{-27}	1.8×10^{-8}	0.96
J1036 − 8317	586.7	0.9	2.6×10^{-27}	6.6×10^{-27}	1.7×10^{-8}	0.74
J1038 + 0032	69.3	6.0	2.1×10^{-28}	7.6×10^{-27}	8.9×10^{-6}	0.59
J1045 − 4509	267.6	0.6	2.1×10^{-27}	4.8×10^{-27}	3.7×10^{-8}	0.91
J1101 − 6101	31.8	7.0	4.2×10^{-26}	2.3×10^{-26}	1.5×10^{-4}	0.62
J1101 − 6424	391.4	2.2	2.2×10^{-28}	6.1×10^{-27}	8.1×10^{-8}	0.6

(Table continued)

TABLE II. *(Continued)*

Pulsar name (J2000)	f_{gw} (Hz)	Distance (kpc)	h_{sd}	$h_0^{95\%}$	$\epsilon^{95\%}$	P-value
J1103 − 5403	589.5	1.7	5.0×10^{-28}	5.4×10^{-27}	2.5×10^{-8}	1
J1125 − 5825	644.7	1.7	2.0×10^{-27}	7.0×10^{-27}	2.8×10^{-8}	0.78
J1125 − 6014	760.3	1.4	7.1×10^{-28}	7.7×10^{-27}	1.8×10^{-8}	0.78
J1125 + 7819	476.0	0.9	$\cdots$	7.3×10^{-27}	2.7×10^{-8}	0.48
J1142 + 0119	394.1	2.2	$\cdots$	1.0×10^{-26}	1.3×10^{-7}	0.067
J1207 − 5050	413.0	1.3	6.9×10^{-28}	8.4×10^{-27}	5.9×10^{-8}	0.17
J1216 − 6410	565.1	1.1	5.0×10^{-28}	5.9×10^{-27}	1.9×10^{-8}	0.92
J1231 − 1411	542.9	0.4	2.9×10^{-27}	9.4×10^{-27}	1.3×10^{-8}	0.29
J1300 + 1240	321.6	0.6	$\cdots$	6.1×10^{-27}	3.4×10^{-8}	0.64
J1302 − 3258	530.4	1.4	7.4×10^{-28}	7.1×10^{-27}	3.4×10^{-8}	0.67
J1302 − 6350	41.9	2.3	7.7×10^{-26}	9.9×10^{-27}	1.2×10^{-5}	0.97
J1312 + 0051	473.0	1.5	7.6×10^{-28}	9.8×10^{-27}	6.1×10^{-8}	0.21
J1327 − 0755	746.8	25.0	$\cdots$	7.9×10^{-27}	3.3×10^{-7}	0.9
J1327 + 3423	48.2	$\cdots$	$\cdots$	1.3×10^{-26}	$\cdots$	0.5
J1337 − 6423	212.2	5.9	1.9×10^{-28}	7.5×10^{-27}	9.3×10^{-7}	0.13
J1400 − 1431	648.5	0.3	5.1×10^{-28}	6.7×10^{-27}	4.0×10^{-9}	0.98
J1411 + 2551	32.0	1.1	8.5×10^{-28}	2.8×10^{-26}	2.9×10^{-5}	0.3
J1412 + 7922	33.8	2.0	9.5×10^{-26}	2.0×10^{-26}	3.3×10^{-5}	0.48
J1420 − 5625	58.6	1.3	8.5×10^{-28}	8.0×10^{-27}	2.9×10^{-6}	0.88
J1421 − 4409	313.2	2.1	3.8×10^{-28}	5.9×10^{-27}	1.2×10^{-7}	0.59
J1431 − 5740	486.6	3.5	2.8×10^{-28}	7.6×10^{-27}	1.1×10^{-7}	0.44
J1435 − 6100	214.0	2.8	4.6×10^{-28}	9.1×10^{-27}	5.3×10^{-7}	0.024
J1439 − 5501	69.8	0.7	2.7×10^{-27}	8.5×10^{-27}	1.1×10^{-6}	0.21
J1446 − 4701	911.3	1.5	1.1×10^{-27}	9.6×10^{-27}	1.6×10^{-8}	0.69
J1453 + 1902	345.3	1.3	8.0×10^{-28}	6.9×10^{-27}	7.0×10^{-8}	0.44
J1455 − 3330	250.4	1.0	1.3×10^{-27}	6.7×10^{-27}	1.0×10^{-7}	0.41
J1502 − 6752	74.8	7.7	3.0×10^{-28}	5.8×10^{-27}	7.5×10^{-6}	0.84
J1513 − 2550	943.8	4.0	6.5×10^{-28}	1.4×10^{-26}	5.7×10^{-8}	0.26
J1514 − 4946	557.2	0.9	1.6×10^{-27}	1.0×10^{-26}	2.9×10^{-8}	0.19
J1518 + 0204A	360.1	8.0	2.8×10^{-28}	5.6×10^{-27}	3.3×10^{-7}	1
J1518 + 4904	48.9	1.0	6.3×10^{-28}	9.7×10^{-27}	3.7×10^{-6}	0.97
J1525 − 5545	176.1	3.1	8.7×10^{-28}	4.9×10^{-27}	4.7×10^{-7}	0.81
J1528 − 3146	32.9	0.8	2.1×10^{-27}	2.5×10^{-26}	1.7×10^{-5}	0.41
J1529 − 3828	235.7	4.3	3.4×10^{-28}	4.5×10^{-27}	3.3×10^{-7}	0.97
J1537 + 1155	52.8	1.1	6.0×10^{-27}	1.3×10^{-26}	4.8×10^{-6}	0.17
J1543 − 5149	972.3	1.1	1.9×10^{-27}	9.2×10^{-27}	1.1×10^{-8}	0.85
J1544 + 4937	926.2	3.0	3.1×10^{-28}	1.7×10^{-26}	5.7×10^{-8}	0.019
J1545 − 4550	559.4	2.2	1.4×10^{-27}	9.5×10^{-27}	6.3×10^{-8}	0.32
J1547 − 5709	466.1	2.7	3.9×10^{-28}	7.8×10^{-27}	9.2×10^{-8}	0.32
J1551 − 0658	281.9	1.3	1.0×10^{-27}	8.5×10^{-27}	1.3×10^{-7}	0.15
J1600 − 3053	555.9	3.0	4.0×10^{-28}	9.9×10^{-27}	9.1×10^{-8}	0.25
J1603 − 7202	134.8	3.4	2.5×10^{-28}	4.5×10^{-27}	8.0×10^{-7}	0.92
J1614 − 2230	634.8	0.7	1.2×10^{-27}	7.6×10^{-27}	1.2×10^{-8}	0.76
J1618 − 3921	166.8	5.5	3.1×10^{-28}	9.3×10^{-27}	1.7×10^{-6}	0.036
J1618 − 4624	337.2	3.0	1.9×10^{-28}	6.1×10^{-27}	1.5×10^{-7}	0.56
J1622 − 6617	84.7	4.0	2.9×10^{-28}	6.0×10^{-27}	3.2×10^{-6}	0.69
J1623 − 2631	180.6	1.8	1.3×10^{-27}	5.0×10^{-27}	2.6×10^{-7}	0.92
J1628 − 3205	622.7	1.2	$\cdots$	7.1×10^{-27}	2.1×10^{-8}	0.79
J1629 − 6902	333.3	1.0	1.1×10^{-27}	6.0×10^{-27}	4.9×10^{-8}	0.79
J1630 + 3734	602.8	1.2	1.1×10^{-27}	7.9×10^{-27}	2.5×10^{-8}	0.53
J1640 + 2224	632.2	1.5	3.4×10^{-28}	1.1×10^{-26}	3.9×10^{-8}	0.17
J1641 + 3627A	192.7	7.1	3.2×10^{-28}	4.3×10^{-27}	7.7×10^{-7}	1

(Table continued)

TABLE II. *(Continued)*

Pulsar name (J2000)	f_{gw} (Hz)	Distance (kpc)	h_{sd}	$h_0^{95\%}$	$\varepsilon^{95\%}$	P-value
J1643 − 1224	432.7	1.2	1.3×10^{-27}	1.1×10^{-26}	6.6×10^{-8}	0.045
J1652 − 4838	528.4	$\cdots$	$\cdots$	9.7×10^{-27}	$\cdots$	0.14
J1653 − 2054	484.4	2.6	5.0×10^{-28}	7.5×10^{-27}	8.0×10^{-8}	0.6
J1658 − 5324	819.9	0.9	1.9×10^{-27}	1.1×10^{-26}	1.4×10^{-8}	0.3
J1705 − 1903	806.4	2.4	9.8×10^{-28}	1.2×10^{-26}	4.0×10^{-8}	0.33
J1708 − 3506	443.9	3.3	3.4×10^{-28}	6.2×10^{-27}	9.9×10^{-8}	0.74
J1709 + 2313	431.9	2.2	1.9×10^{-28}	6.4×10^{-27}	7.1×10^{-8}	0.68
J1713 + 0747	437.6	1.0	1.1×10^{-27}	7.0×10^{-27}	3.5×10^{-8}	0.59
J1719 − 1438	345.4	0.3	2.6×10^{-27}	8.0×10^{-27}	2.1×10^{-8}	0.25
J1721 − 2457	572.0	1.4	$\cdots$	8.0×10^{-27}	3.1×10^{-8}	0.59
J1727 − 2946	73.8	1.9	1.3×10^{-27}	9.3×10^{-27}	3.0×10^{-6}	0.2
J1729 − 2117	30.2	1.0	1.3×10^{-27}	2.6×10^{-26}	2.7×10^{-5}	0.83
J1730 − 2304	246.2	0.5	2.0×10^{-27}	5.8×10^{-27}	4.2×10^{-8}	0.64
J1732 − 5049	376.5	1.9	6.2×10^{-28}	4.6×10^{-27}	5.8×10^{-8}	1
J1737 − 0811	479.0	0.2	5.4×10^{-27}	8.4×10^{-27}	7.3×10^{-9}	0.44
J1738 + 0333	341.9	1.5	1.1×10^{-27}	7.1×10^{-27}	8.5×10^{-8}	0.44
J1741 + 1351	533.7	1.1	2.1×10^{-27}	6.4×10^{-27}	2.3×10^{-8}	0.9
J1744 − 1134	490.9	0.4	2.6×10^{-27}	1.1×10^{-26}	1.8×10^{-8}	0.087
J1745 − 0952	103.2	0.2	7.5×10^{-27}	5.7×10^{-27}	1.2×10^{-7}	0.82
J1745 + 1017	754.1	1.2	6.0×10^{-28}	1.1×10^{-26}	2.2×10^{-8}	0.38
J1747 − 4036	1215.4	7.2	2.9×10^{-28}	2.1×10^{-26}	9.8×10^{-8}	0.036
J1748 − 2446A	173.0	6.9	3.3×10^{-28}	5.3×10^{-27}	1.2×10^{-6}	0.76
J1748 − 3009	206.5	5.0	$\cdots$	8.0×10^{-27}	9.0×10^{-7}	0.13
J1750 − 2536	57.6	3.2	5.1×10^{-28}	8.9×10^{-27}	8.2×10^{-6}	0.74
J1751 − 2857	510.9	1.1	1.2×10^{-27}	6.3×10^{-26}	2.5×10^{-7}	0.088
J1753 − 1914	31.8	2.9	1.6×10^{-27}	2.6×10^{-26}	7.2×10^{-5}	0.56
J1753 − 2240	21.0	3.2	8.0×10^{-28}	1.7×10^{-25}	1.2×10^{-3}	0.33
J1755 − 3716	156.4	8.2	1.5×10^{-28}	6.4×10^{-27}	2.0×10^{-6}	0.41
J1756 − 2251	70.3	0.7	6.6×10^{-27}	8.8×10^{-27}	1.2×10^{-6}	0.41
J1757 − 1854	93.0	19.6	4.6×10^{-28}	1.2×10^{-26}	2.5×10^{-5}	0.018
J1757 − 5322	225.5	0.9	1.5×10^{-27}	6.0×10^{-27}	1.0×10^{-7}	0.45
J1801 − 1417	551.7	1.1	7.4×10^{-28}	8.9×10^{-27}	3.0×10^{-8}	0.41
J1801 − 3210	268.3	6.1	$\cdots$	6.2×10^{-27}	5.0×10^{-7}	0.52
J1802 − 2124	158.1	0.8	2.5×10^{-27}	6.4×10^{-27}	1.8×10^{-7}	0.49
J1804 − 0735	86.6	7.8	2.9×10^{-28}	7.8×10^{-27}	7.7×10^{-6}	0.39
J1804 − 2717	214.1	0.8	1.9×10^{-27}	6.1×10^{-27}	1.0×10^{-7}	0.51
J1807 − 2459A	653.7	3.0	7.6×10^{-28}	9.4×10^{-27}	6.3×10^{-8}	0.41
J1809 − 1917	24.2	3.3	1.4×10^{-25}	5.6×10^{-26}	3.0×10^{-4}	0.85
J1810 + 1744	1202.8	2.4	5.5×10^{-28}	1.2×10^{-26}	1.8×10^{-8}	0.82
J1810 − 2005	60.9	3.5	2.9×10^{-28}	8.5×10^{-27}	7.6×10^{-6}	0.69
J1811 − 2405	751.7	1.8	9.9×10^{-28}	7.2×10^{-27}	2.2×10^{-8}	0.98
J1813 − 1749	44.7	6.2	2.2×10^{-25}	1.1×10^{-26}	3.1×10^{-5}	0.89
J1813 − 2621	451.5	3.2	$\cdots$	5.4×10^{-27}	8.0×10^{-8}	0.98
J1821 + 0155	59.2	1.7	4.3×10^{-28}	9.1×10^{-27}	4.2×10^{-6}	0.92
J1823 − 3021A	367.6	7.9	2.9×10^{-28}	8.6×10^{-27}	4.8×10^{-7}	0.15
J1824 − 2452A	654.8	5.5	4.1×10^{-28}	8.7×10^{-27}	1.1×10^{-7}	0.55
J1825 − 0319	439.2	3.9	2.6×10^{-28}	5.5×10^{-27}	1.0×10^{-7}	0.98
J1826 − 2415	425.9	2.7	5.7×10^{-28}	7.0×10^{-27}	10.0×10^{-8}	0.53
J1828 − 1101	27.8	4.8	7.7×10^{-26}	3.2×10^{-26}	1.9×10^{-4}	0.91
J1829 + 2456	48.8	0.9	10.0×10^{-28}	1.4×10^{-26}	5.2×10^{-6}	0.57
J1832 − 0836	735.5	1.6	$\cdots$	1.4×10^{-26}	3.8×10^{-8}	0.093
J1833 − 0827	23.4	4.5	5.9×10^{-26}	6.1×10^{-26}	4.7×10^{-4}	0.91

(Table continued)

TABLE II. *(Continued)*

Pulsar name (J2000)	f_{gw} (Hz)	Distance (kpc)	h_{sd}	$h_0^{95\%}$	$\epsilon^{95\%}$	P-value
J1835 − 0114	390.9	3.5	2.7×10^{-28}	6.4×10^{-27}	1.4×10^{-7}	0.71
J1838 − 0655	28.4	6.6	1.0×10^{-25}	3.4×10^{-26}	2.6×10^{-4}	0.72
J1840 − 0643	56.2	5.0	2.6×10^{-28}	8.5×10^{-27}	1.3×10^{-5}	0.82
J1841 + 0130	67.2	4.2	3.2×10^{-27}	1.2×10^{-26}	1.1×10^{-5}	0.037
J1843 − 1113	1083.6	1.3	1.4×10^{-27}	2.2×10^{-26}	2.2×10^{-8}	0.019
J1843 − 1448	365.5	3.5	$\cdots$	8.3×10^{-27}	2.0×10^{-7}	0.23
J1849 − 0001	51.9	7.0	7.0×10^{-26}	1.5×10^{-26}	3.8×10^{-5}	0.08
J1853 + 1303	488.8	1.3	8.9×10^{-28}	1.2×10^{-26}	6.1×10^{-8}	0.058
J1856 + 0245	24.7	6.3	1.1×10^{-25}	5.7×10^{-26}	5.6×10^{-4}	0.69
J1857 + 0943	373.0	1.2	1.2×10^{-27}	7.2×10^{-27}	5.8×10^{-8}	0.48
J1902 − 5105	1147.8	1.6	1.1×10^{-27}	1.3×10^{-26}	1.5×10^{-8}	0.59
J1903 + 0327	930.3	6.1	3.9×10^{-28}	1.4×10^{-26}	9.3×10^{-8}	0.24
J1903 − 7051	555.9	0.9	1.3×10^{-27}	6.7×10^{-27}	1.9×10^{-8}	0.77
J1904 + 0412	28.1	4.6	2.2×10^{-28}	2.9×10^{-26}	1.6×10^{-4}	0.98
J1905 + 0400	528.5	1.1	8.0×10^{-28}	7.3×10^{-27}	2.6×10^{-8}	0.68
J1909 − 3744	678.6	1.1	6.6×10^{-28}	8.1×10^{-27}	1.9×10^{-8}	0.64
J1910 + 1256	401.3	1.5	7.2×10^{-28}	8.1×10^{-27}	7.2×10^{-8}	0.29
J1911 − 1114	551.6	1.1	1.3×10^{-27}	1.2×10^{-26}	4.0×10^{-8}	0.067
J1911 + 1347	432.3	1.4	1.1×10^{-27}	7.1×10^{-27}	4.9×10^{-8}	0.54
J1913 + 1011	55.7	4.6	5.3×10^{-26}	8.6×10^{-27}	1.2×10^{-5}	0.82
J1914 + 0659	108.0	8.5	1.2×10^{-28}	8.1×10^{-27}	5.6×10^{-6}	0.23
J1915 + 1606	33.9	5.2	1.9×10^{-27}	2.6×10^{-26}	1.1×10^{-4}	0.21
J1918 − 0642	261.6	1.1	1.3×10^{-27}	6.7×10^{-27}	1.0×10^{-7}	0.45
J1923 + 2515	528.0	1.2	9.1×10^{-28}	1.0×10^{-26}	4.1×10^{-8}	0.15
J1925 + 1720	26.4	5.1	5.9×10^{-26}	7.0×10^{-26}	4.8×10^{-4}	0.039
J1928 + 1746	29.1	4.3	8.2×10^{-26}	3.4×10^{-26}	1.6×10^{-4}	0.54
J1933 − 6211	564.4	0.7	1.1×10^{-27}	6.9×10^{-27}	1.3×10^{-8}	0.66
J1935 + 2025	25.0	4.6	1.5×10^{-25}	4.9×10^{-26}	3.4×10^{-4}	0.66
J1939 + 2134	1283.9	4.8	1.4×10^{-27}	1.4×10^{-26}	4.0×10^{-8}	0.59
J1943 + 2210	393.4	6.8	1.6×10^{-28}	6.4×10^{-27}	2.6×10^{-7}	0.62
J1944 + 0907	385.7	1.2	7.4×10^{-28}	6.1×10^{-27}	4.8×10^{-8}	0.75
J1946 + 3417	630.9	6.9	6.5×10^{-29}	9.3×10^{-27}	1.5×10^{-7}	0.34
J1946 − 5403	737.8	1.1	7.0×10^{-28}	7.1×10^{-27}	1.4×10^{-8}	0.89
J1949 + 3106	152.2	7.5	2.9×10^{-28}	5.8×10^{-27}	1.8×10^{-6}	0.67
J1950 + 2414	464.6	7.3	2.4×10^{-28}	6.8×10^{-27}	2.2×10^{-7}	0.67
J1952 + 3252	50.6	3.0	1.0×10^{-25}	1.3×10^{-26}	1.4×10^{-5}	0.22
J1955 + 2527	410.4	8.2	1.5×10^{-28}	7.7×10^{-27}	3.5×10^{-7}	0.36
J1955 + 2908	326.1	6.3	2.9×10^{-28}	6.6×10^{-27}	3.7×10^{-7}	0.46
J2007 + 2722	81.6	7.1	7.1×10^{-28}	1.1×10^{-26}	1.1×10^{-5}	0.037
J2010 − 1323	382.9	1.2	5.3×10^{-28}	8.4×10^{-27}	6.3×10^{-8}	0.22
J2017 + 0603	690.6	1.4	9.6×10^{-28}	8.9×10^{-27}	2.5×10^{-8}	0.6
J2019 + 2425	508.3	1.2	4.4×10^{-28}	5.4×10^{-26}	2.3×10^{-7}	0.046
J2022 + 2534	755.9	$\cdots$	$\cdots$	1.2×10^{-26}	$\cdots$	0.2
J2033 + 1734	336.2	1.7	5.5×10^{-28}	5.2×10^{-27}	7.6×10^{-8}	0.92
J2039 − 3616	610.7	1.7	7.6×10^{-28}	7.6×10^{-27}	3.3×10^{-8}	0.65
J2043 + 2740	20.8	1.5	6.3×10^{-26}	1.7×10^{-25}	5.6×10^{-4}	0.32
J2045 + 3633	63.1	5.6	6.2×10^{-28}	9.1×10^{-27}	1.2×10^{-5}	0.34
J2047 + 1053	466.6	2.8	6.4×10^{-28}	7.0×10^{-27}	8.5×10^{-8}	0.69
J2053 + 4650	158.9	3.8	7.8×10^{-28}	4.6×10^{-27}	6.6×10^{-7}	0.92
J2055 + 3829	957.3	4.6	1.1×10^{-28}	1.2×10^{-26}	5.8×10^{-8}	0.36
J2124 − 3358	405.6	0.4	2.3×10^{-27}	8.0×10^{-27}	2.0×10^{-8}	0.28
J2129 − 5721	536.7	7.0	2.6×10^{-28}	7.8×10^{-27}	1.8×10^{-7}	0.41

(Table continued)

TABLE II. *(Continued)*

Pulsar name (J2000)	f_{gw} (Hz)	Distance (kpc)	h_{sd}	$h_0^{95\%}$	$\epsilon^{95\%}$	P-value
J2144 − 5237	396.7	1.7	6.5×10^{-28}	6.0×10^{-27}	6.0×10^{-8}	0.63
J2145 − 0750	124.6	0.8	1.3×10^{-27}	6.5×10^{-27}	3.3×10^{-7}	0.52
J2150 − 0326	569.7	$\cdots$	$\cdots$	8.9×10^{-27}	$\cdots$	0.46
J2205 + 6012	828.0	3.5	6.5×10^{-28}	8.9×10^{-27}	4.3×10^{-8}	0.7
J2214 + 3000	641.2	0.6	2.7×10^{-27}	6.8×10^{-27}	9.3×10^{-9}	0.92
J2222 − 0137	60.9	0.3	2.0×10^{-27}	7.2×10^{-27}	5.0×10^{-7}	0.91
J2229 + 2643	671.6	1.8	3.1×10^{-28}	1.1×10^{-26}	4.2×10^{-8}	0.19
J2229 + 6114	38.7	3.0	3.3×10^{-25}	1.3×10^{-26}	2.4×10^{-5}	0.8
J2234 + 0611	559.2	1.5	8.2×10^{-28}	1.3×10^{-26}	5.9×10^{-8}	0.071
J2234 + 0944	551.4	0.8	1.9×10^{-27}	7.6×10^{-27}	1.9×10^{-8}	0.68
J2235 + 1506	33.5	1.5	6.5×10^{-28}	2.3×10^{-26}	2.9×10^{-5}	0.53
J2236 − 5527	289.5	2.0	4.6×10^{-28}	5.0×10^{-27}	1.2×10^{-7}	0.78
J2241 − 5236	914.6	1.1	1.2×10^{-27}	1.4×10^{-26}	1.7×10^{-8}	0.097
J2256 − 1024	871.6	1.3	1.3×10^{-27}	1.6×10^{-26}	2.7×10^{-8}	0.057
J2302 + 4442	385.2	0.9	1.5×10^{-27}	7.0×10^{-27}	3.9×10^{-8}	0.39
J2317 + 1439	580.5	2.2	3.3×10^{-28}	7.5×10^{-27}	4.6×10^{-8}	0.72
J2322 + 2057	415.9	1.0	6.5×10^{-28}	6.2×10^{-27}	3.4×10^{-8}	0.77
J2322 − 2650	577.5	0.2	1.2×10^{-27}	7.0×10^{-27}	4.6×10^{-9}	0.78

[1] The LIGO Scientific Collaboration, Advanced LIGO, Classical Quantum Gravity **32,** 074001 (2015).

[2] F. Acernese *et al.*, Advanced Virgo: A second-generation interferometric gravitational wave detector, Classical Quantum Gravity **32,** 024001 (2015).

[3] The LIGO Scientific and Virgo Collaborations, Gravitational waves from known pulsars: Results from the initial detector era, Astrophys. J. **785,** 119 (2014).

[4] K. Glampedakis and L. Gualtieri, Gravitational waves from single neutron stars: An advanced detector era survey, in *The Physics and Astrophysics of Neutron Stars*, edited by L. Rezzolla, P. Pizzochero, D. I. Jones, N. Rea, and I. Vidaña (Springer International Publishing, Cham, 2018).

[5] P. Jaranowski, A. Królak, and B. F. Schutz, Data analysis of gravitational-wave signals from spinning neutron stars: The signal and its detection, Phys. Rev. D **58,** 063001 (1998).

[6] D. I. Jones, Learning from the frequency content of continuous gravitational wave signals, arXiv:2111.08561.

[7] O. J. Piccinni, Status and perspectives of continuous gravitational wave searches, Galaxies **10,** 72 (2022).

[8] B. P. Abbott *et al.*, First search for gravitational waves from known pulsars with advanced LIGO, Astrophys. J. **839,** 12 (2017).

[9] The LIGO Scientific, Virgo, and KAGRA Collaborations, Searches for gravitational waves from known pulsars at two harmonics in the second and third LIGO-Virgo observing runs, Astrophys. J. Lett. **935** (2022).

[10] P. Astone, S. D'Antonio, S. Frasca, and C. Palomba, A method for detection of known sources of continuous gravitational wave signals in non-stationary data, Classical Quantum Gravity **27,** 194016 (2010).

[11] P. Astone, A. Colla, S. D'Antonio, S. Frasca, C. Palomba, and R. Serafinelli, Method for narrow-band search of continuous gravitational wave signals, Phys. Rev. D **89,** 062008 (2014).

[12] M. Pitkin, C. Messenger, and X. Fan, Hierarchical Bayesian method for detecting continuous gravitational waves from an ensemble of pulsars, Phys. Rev. D **98,** 063001 (2018).

[13] X. Fan, Y. Chen, and C. Messenger, Method to detect gravitational waves from an ensemble of known pulsars, Phys. Rev. D **94,** 084029 (2016).

[14] M. Buono, R. De Rosa, L. D'Onofrio, L. Errico, C. Palomba, O. Piccinni, and V. Sequino, A method for detecting continuous gravitational wave signals from an ensemble of known pulsars, Classical Quantum Gravity **38,** 135021 (2021).

[15] L. D'Onofrio, R. De Rosa, L. Errico, C. Palomba, V. Sequino, and L. Trozzo, 5n-vector ensemble method for detecting gravitational waves from known pulsars, Phys. Rev. D **105,** 063012 (2022).

[16] O. J. Piccinni, P. Astone, S. D'Antonio, S. Frasca, G. Intini, P. Leaci, S. Mastrogiovanni, A. L. Miller, C. Palomba, and A. Singhal, A new data analysis framework for the search of continuous gravitational wave signals, Classical Quantum Gravity **36,** 015008 (2019).

[17] *Observation time* refers to the amount of data; that is, the time span not considering the periods where the detector was in NO-science mode.

[18] The LIGO and Virgo Collaborations, Searches for gravitational waves from known pulsars at two harmonics in 2015-2017 LIGO data, Astrophys. J. **879,** 10 (2019).

[19] E. Thrane and C. Talbot, An introduction to bayesian inference in gravitational-wave astronomy: Parameter estimation, model selection, and hierarchical models, Publ. Astron. Soc. Aust. **36,** e010 (2019).

[20] Gravitational Wave Open Science Center, https://www.gw-openscience.org/O3/index/.

[21] The ephemerides and the rotational/orbital parameters may be obtainable on request at the discretion of the individual EM pulsar groups from the above-mentioned observatories.

[22] M. Amiri *et al.*, The CHIME pulsar project: System overview, Astrophys. J. Suppl. Ser. **255,** 5 (2021).

[23] M. Bailes *et al.*, The MeerKAT Telescope as a pulsar facility: System verification and early science results from MeerTime, Pub. Astron. Soc. Aust. **37,** e028 (2020).

[24] F. Jankowski, M. Bailes, W. van Straten, E. F. Keane, C. Flynn, E. D. Barr, T. Bateman, S. Bhandari, M. Caleb, D. Campbell-Wilson, W. Farah, A. J. Green, R. W. Hunstead, A. Jameson, S. Osłowski, A. Parthasarathy, P. A. Rosado, and V. Venkatraman Krishnan, The UTMOST pulsar timing programme I: Overview and first results, Mon. Not. R. Astron. Soc. **484,** 3691 (2019).

[25] M. E. Lower, M. Bailes, R. M. Shannon, S. Johnston, C. Flynn, S. Osłowski, V. Gupta, W. Farah, T. Bateman, A. J. Green, R. Hunstead, A. Jameson, F. Jankowski, A. Parthasarathy, D. C. Price, A. Sutherland, D. Temby, and V. Venkatraman Krishnan, The UTMOST pulsar timing programme—II. Timing noise across the pulsar population, Mon. Not. R. Astron. Soc. **494,** 228 (2020).

[26] D. Nice, P. Demorest, I. Stairs, R. Manchester, J. Taylor, W. Peters, J. Weisberg, A. Irwin, N. Wex, and Y. Huang, TEMPO: Pulsar timing data analysis (2015), ascl:1509.002.

[27] R. T. Edwards, G. B. Hobbs, and R. N. Manchester, TEMPO2, A new pulsar timing package—II. The timing model and precision estimates, Mon. Not. R. Astron. Soc. **372,** 1549 (2006).

[28] G. Hobbs, R. Edwards, and R. Manchester, TEMPO2: A new pulsar timing package, Chin. J. Astron. Astrophys. Suppl. **6,** 189 (2006).

[29] G. Hobbs, F. Jenet, K. J. Lee, J. P. W. Verbiest, D. Yardley, R. Manchester, A. Lommen, W. Coles, R. Edwards, and C. Shettigara, TEMPO2: A new pulsar timing package—III. Gravitational wave simulation, Mon. Not. R. Astron. Soc. **394,** 1945 (2009).

[30] ATNF Pulsar Catalogue, catalogue version 1.61, https://www.atnf.csiro.au/research/pulsar/psrcat/.

[31] J. M. Yao, R. N. Manchester, and N. Wang, A new electron-density model for estimation of pulsar and FRB Distances, Astrophys. J. **835,** 29 (2017).

[32] J. M. Cordes and T. J. W. Lazio, NE2001.I: A new model for the galactic distribution of free electrons and its fluctuations, in *Milky Way Surveys: The Structure and Evolution of our Galaxy*, Astronomical Society of the Pacific Conference Series Vol. 317, edited by D. Clemens, R. Shah, and T. Brainerd (2004), p. 211, https://ui.adsabs.harvard.edu/abs/2004ASPC..317..211C.

[33] B. Haskell and A. Melatos, Models of pulsar glitches, Int. J. Mod. Phys. D **24,** 1530008 (2015).

[34] P. Leaci and R. Prix, Directed searches for continuous gravitational waves from binary systems: Parameter-space metrics and optimal Scorpius X-1 sensitivity, Phys. Rev. D **91,** 102003 (2015).

[35] J. Condon and S. Ransom, *Essential Radio Astronomy*, Princeton Series in Modern Observational Astronomy (Princeton University Press, Princeton, NJ, 2016).

[36] F. De Lillo, J. Suresh, and A. L. Miller, Stochastic gravitational-wave background searches and constraints on neutron-star ellipticity, Mon. Not. R. Astron. Soc. **513,** 1105 (2022).

[37] D. Agarwal, J. Suresh, V. Mandic, A. Matas, and T. Regimbau, Targeted search for the stochastic gravitational-wave background from the galactic millisecond pulsar population, Phys. Rev. D **106,** 043019 (2022).

[38] B. P. Abbott *et al.*, All-sky search for continuous gravitational waves from isolated neutron stars using Advanced LIGO and Advanced Virgo O3 data, Phys. Rev. D **106,** 102008 (2022).

[39] G. Woan, M. D. Pitkin, B. Haskell, D. I. Jones, and P. D. Lasky, Evidence for a minimum ellipticity in millisecond pulsars, Astrophys. J. Lett. **863,** L40 (2018).

[40] https://www.gw-openscience.org/.

[41] www.westgrid.ca.

[42] www.computecanada.ca.

[43] P. Astone, A. Colla, S. D'Antonio, S. Frasca, and C. Palomba, Coherent search of continuous gravitational wave signals: Extension of the 5-vectors method to a network of detectors, J. Phys. Conf. Ser. **363,** 012038 (2012).

[44] C. Biwer *et al.*, Validating gravitational-wave detections: The Advanced LIGO hardware injection system, Phys. Rev. D **95,** 062002 (2017).

[45] O3 continuous wave hardware injections, https://www.gw-openscience.org/O3/o3_inj/, accessed: 2022-07-20.

[46] The coherence is a number between 0 and 1 that measures the resemblance between the shape of the expected signal and the data. Differently form the p-value, the noise distribution of the coherence is not flat between 0 and 1 (see [10]). It is a supplemental parameter to show the significance of the detection.